PIEZOELECTRIC ACTIVE SENSOR AND ELECTRIC IMPEDANCE APPROACH FOR STRUCTURAL DYNAMIC MEASUREMENT

by

Fanping Sun

Thesis submitted to the Faculty of the
Virginia Polytechnic Institute and State University
in partial fulfillment of the requirements for the degree of
Master of Science
in
Mechanical Engineering

APPROVED

Dr. Craig A. Rogers, Chairman

Dr. Victor Giurgiutiu

Dr. Will R. Saunders

June, 1996
Blacksburg, Virginia

Keywords: Piezoelectric, Active sensing, Actuation, Electric Impedance, Structural Dynamic Measurement

PIEZOELECTRIC ACTIVE SENSOR AND ELECTRIC IMPEDANCE APPROACH FOR STRUCTURAL DYNAMIC MEASUREMENT

by

Fanping Sun

Committee Chairman: Dr. Craig A. Rogers

Mechanical Engineering

(ABSTRACT)

The increasing use of piezoelectric material in the last decade has led to the new discovery that piezoelectric devices may be used not only as sensors or actuators individually, but also as a sensor and actuator at the same time. This bi-directional phenomenon greatly expands the utility of piezoelectric devices, especially in the area of smart material systems and structures, such as structural dynamic measurement analysis, structural damage detection, active structural vibration and acoustic control, etc.

Presented in this thesis is a new electromechanical approach for structural dynamic analysis. It uses PZT patches bonded on structures as active piezoelectric sensors, and acquires the structural information by measuring the electric admittance of the sensors. Because of the electromechanical coupling, the electric admittance is mechanically modulated by the structural dynamics through the piezoelectric effect. The structural

dynamic characteristics can then be extracted using a mathematical model governing the interaction of PZT actuators and structures.

In this thesis, a multi-input, multi-output mathematical model is derived based on the one-dimensional constitutive law of the PZT and the mechanical impedance approach. The model yields explicit expressions of structural mechanical mobility in terms of the measured electric admittance. Applications of the approach in smart structures are presented in the area of mechanical frequency response function extraction, structural modal analysis, and structural health monitoring. As a general issue related to the application of PZT sensor-actuators in smart structures, the energy conversion efficiency of PZT actuators has also been experimentally investigated.

Acknowledgments

I wish to express my deep gratitude to Dr. Craig Rogers for his understanding and support of my desire to complete a degree at Virginia Tech, and for giving me the opportunity as a part-time graduate student to perform this work. I would also like to thank him for providing the technical guidance which greatly helped me to be productive and successful in my research at the Center for Intelligent Material Systems and Structures.

The support of my extended family has been unwavering. To all of my family I thank you from my heart for believing in me. Although I am halfway around the world far away, be sure to know that my thoughts are with you.

I wish to thank my former colleagues and friends, Chen Liang and Zaffir Chaudhry, for their support and help in my four years of research. I also wish to express my special thanks to Ms. Beth Howell for her kind proofreading of my thesis.

To my wife Ping Lu goes my deepest gratitude. She has never stopped giving me her encouragement to complete a degree in the USA. For her understanding, support, and patience, I am eternally thankful.

Table of Contents

List of Figures

List of Tables

Chapter 1

Introduction

The current status of piezoelectric material and devices for sensing or actuation is briefly discussed. The recently-developed technique using PZT as sensors and actuators at the same time for active control is reviewed. A new concept is presented whereby the coupled electric impedance of a PZT gives it utility as an active sensing information for structural dynamic measurement.

1.1 Piezoelectricity and its Applications

It has been more than a century since the discovery of the piezoelectric effect by Pierre and Jacques Curie in 1880. Piezoelectricity is a phenomenon in which certain crystalline substances develop an electric field when subjected to pressure force, or, conversely, exhibit a mechanical deformation when subjected to an electric field. This reciprocal coupling between mechanical and electrical energy renders piezoelectric materials useful in many applications.

The existence of this effect has been proven in many different materials. Only very few, however, have been found suitable for practical applications. Lead-Zirconate-Titanate,

usually abbreviated as PZT, is one of the most commonly used piezoelectric ceramics. In addition to its piezoelectric characteristics, PZT exhibits excellent properties under normal working conditions, such as a large range of linearity in piezoelectric effect, long-term temperature stability, and low internal friction loss coefficient. In the manufacture of piezoceramics, a suitable dielectric material is fabricated into the desired shape, and electrodes are applied. The piezoceramic element is then heated to an elevated temperature while in the presence of a strong dc electric field. This polarizes or poles the ceramic (aligns the molecular dipoles of the ceramic in the direction of the applied field) and provides it with piezoelectric properties.

Because of its distinct characteristics, PZT ceramics have been widely employed in many scientific and engineering fields for both sensors and actuators. Typical applications include three categories: The first category include ultrasonic acoustic transduction devices, which are commonly used in non-destructive evaluation (NDE) and medical examination. Sonar probes are another important application. In this category, piezoelectric devices are used as both wave emitters and receivers, but not at the same time. The devices operate in very much the same way as radar does. It sends out an impulsive signal as an actuator and then is electronically switched to receiving mode for reception of the signal bouncing back. In the second, category, the piezoelectric material is used as either a sensor or an actuator individually, such as piezoelectric accelerometers, force gages, mechanical impedance heads, or stack actuators. The third category of

application is electromechanical resonators. This category exploits the high frequency stability of a piezoelectric material when operating in an oscillation mode. Typical applications are frequency stabilizers, signal filters and oscillating signal sources, which are commonly used in electronic circuitry.

As solid-state electromechanical transduction devices, piezoelectric materials possess many superiority over other transduction elements. They are light in weight, low in power consumption, fast in response, and high in energy conversion efficiency. Because of these characteristics, piezoelectric transducers have been increasingly adopted in aerospace engineering, medical diagnostics, automobile industries, civil engineering, nuclear industries, etc.

1.2 Simultaneous Actuation and Sensing by PZT

New applications of piezoelectric devices for simultaneous actuation and sensing have been of great interest in both academics and industries in the last few years. The theoretical basis of this type of application is the reciprocity of the piezoelectric effect. That is, the applied electric field results in a mechanical deformation of the PZT. At the same time, this deformation also creates an additional electrical charge as a feed-back. This bi-directional phenomenon exists in many electromechanical transduction devices. A dc electric motor is, in actuality, an electromechanical coupler between electric voltage,

current, rotational speed, and output torque. The electric current flowing in the motor under a constant voltage is a function of the shaft rotational speed, and the speed is in turn a function of the load, or the resistance torque. Therefore, the electric current can be taken as a sensor signal for the level of the load. An electromagnetic shaker, or a voice coil is similar, except, in this case, the mechanical quantities are the force and linear velocity, rather than the rotational speed and torque. This effect has been successfully adopted in the automatic control of the electrical driving system for stabilizing the output in constantly-varying working conditions. An example includes the constant RPM control of the main shaft of a lathe machine. The fluctuation of the shaft RMS due to the unevenness of the cutting tool feeding can be monitored by sensing the electric current of the motor driving the machine, rather than by monitoring the RPM of the shaft directly with a tachometer. The self-sensing by a coil-type actuator through velocity feedback for active vibration control is also reported (Okada et al, 1995). A similar concept has been developed and used in solid-state piezoelectric devices for structural control purposes. The piezoelectric collocated sensor-actuator has been intensively investigated in the last few years (Dosch and Inman, 1991; Anderson and Hagood, 1992; Lee, et al., 1991). The technique of using a single piece of piezoelectric material to concurrently actuate and sense the structural response in a closed loop has been developed. The theoretical background of this approach is that the electric current flowing through a piezoelectric interacting with a structure is proportional to the time rate of the mechanical strain, or the vibration velocity of the structure. By sensing the current, separating the mechanicaly-

induced portion with a differential circuit and feeding it back to the input commanding voltage in an appropriate phase and magnitude, a significant increase in the effective damping of the structure can be achieved. This is similar to the electromagnetic damping resulting from electromagnetic induction when a closed-circuit conductor is moving perpendicular to the magnetic flux, as used in many galvanometers to reduce the overshooting of the indication needles. Proper selection of the feed-back, such as rate or position feed-back and the frequency band filtering, can suppress the vibration modes of the structure selectively while the actuation authority of the piezoelectric is not compromised. The motivation behind the technique is that such a self-sensing actuator will be truly collocated and has a numbers of advantages in active vibration control of structures. The technique has been successfully implemented in a cantilever beam with a closed-loop feed-back, and a significant increase in the effective damping has been achieved in the first few bending modes.

1.3 Coupled Electric Impedance Approach — Active Sensing

A novel approach has recently been developed (Sun, Liang and Rogers, 1995) of utilizing the electric impedance of PZT active sensors for structural dynamic measurement. The electromechanical coupling of a piezoceramic sensor embedded in a structure allows not only for collocated sensing and actuation in control, but also for structural dynamic measurement as well. As described in the previous section, the current flowing through a

piezoelectric interacting with a structure is modulated by the structural response, or the rate of strain, and the actuation force is commanded by the voltage applied to the piezoelectrics. Therefore, the electric impedance of the piezoelectric, which is defined as the ratio of the voltage to the current, supplies information about the mechanical Frequency Response Function (FRF) of the structure. In other words, the electric impedance of the actuator embedded in a structure is a mapping of the dynamic characteristics of the structure. The approach is similar to that for the collocated sensor-actuator in nature, but is aimed at acquiring the structural properties rather than at improving the effective damping through feed-back control. As the PZTs actively interrogate the structural characteristics without additional excitation source, it is appropriate to call them active sensors.

This work was originally started as an effort to develop an alternative approach for modal testing of small and flexible structures (Sun, Liang and Rogers, 1994). The original work was also limited to the acquisition of point mobility as it used a single collocated active sensor and a single input model. Later, with a multi-input, multi-output model, the technique was successfully expanded to the acquisition of both point and transfer mobility (Sun, Liang and Rogers, 1995). This marks the complete evolution of this research as it provides a new method for structural dynamic measurement with not only the features of conventional approaches but also many unsurpassed advantages. Similar analytical work has also been conducted (Cole, Saunders and Robertsaw, 1994, 1995) independently on

the structural modal analysis using piezoelectric elements. In this work, a fundamental relation between modal analysis techniques for conventional structures and piezostructures is developed by means of electromechanical coupling matrix (EMC). This enables the modal testing of piezostructures to take place within the existing framework of modal analysis.

This thesis is a summary of the author's previous work on this new approach. The central focus is the electromechanical modeling through which explicit relations between the measured electric admittance and the mechanical mobility of the structure can be derived. The structural modal testing using this electromechanical approach is discussed as a major supporting section. However, only some features uniquely associated with this approach are included; the conventional methods using FRF for modal analysis are not covered in the thesis. Structural health monitoring is presented as an excellent application of this electromechanical approach. Finally, as a general issue related to the application of PZT actuators in smart structures, the energy conversion coefficients of a PZT stack actuator were investigated.

Chapter 2

Structural Mechanical Mobility Acquisition by Electric Impedance Measurement

This chapter presents the major theoretical background of the technique for acquiring structural Frequency Response Function (FRF) via measurement of the electric impedance of piezoceramic (PZT) actuators.

A multi-input mechanical impedance model governing the electromechanical interaction of PZT actuators with structures has been derived. Both the point FRF of single location and the transfer FRF between two locations on a structure can be extracted from measured electric impedance. The concept of measuring the "coupled impedance" of a single PZT sensor and two PZT sensors in parallel is presented and used to derive the transfer FRF of the structure. The model takes into account the mechanical impedance of the actuator. This allows for the removal of the stiffening effect from the extracted FRF. The relation between the in-plane FRF and the rotational FRF are discussed. An example of extracting in-plane structural FRF of a free-free aluminum beam by surface-bonded PZT sensors is given.

2.1 Motivation

Structural Frequency Response Function acquisition is the key and fundamental portion of structural dynamic analysis, system identification, and active vibration control. Numerous efforts have been devoted to the acquisition of accurate and reliable FRF in the past. Available techniques include the most conventional and popularly used piezoceramic accelerometers, force gages, electromagnetic shakers and multi-channel signal analyzer schemes. More technologically advanced approaches include the use of noncontact sensing such as eddy current sensors and optical fiber displacement sensors. The most state-of-the-art technique for acquiring structural FRF is the Laser Doppler Vibrometer-based automated FRF scanning system (Agee and Mitchell, 1992).

One of the major issues in structural FRF acquisition is the effect of mass loading and stiffening of transducers on the structure's dynamic characteristics. This issue is critical when dealing with light and flexible structures as the attachment of conventional transducers onto the structure may result in considerable errors in the obtained FRF. Noncontact sensing solves the problem to some extent, but the effect of shaking facility and force gage is still a concern. In addition, the entire process of acquiring FRF always requires a set of sophisticated equipment, such as a multi-channel signal analyzer, power amplifiers for shakers and various types of signal conditioners for transducers.

A piezoceramic patch, on the other hand, may serve as both a sensor and an actuator at the same time as a result of the piezoelectric effect and its converse. When bonded to a structure and driven by an alternating voltage, the PZT imposes a forcing function on the structure through its longitudinal expansion and contraction, causing the structure to vibrate. This structural vibration then in turn "modulates" the capacitative current flowing in the patch. Consequently, the electric admittance of the bonded patch, defined as the ratio of the current to the voltage, is physically in the same position as its mechanical counterparts, such as mobility, in representing the transfer characteristics of a structure between the excitation and the response. Previous work has demonstrated the feasibility of conducting structural modal analysis with PZT collocated actuator-sensors based on the measurement of electric impedance (Sun and Rogers, 1994). The results have shown many advantages of this approach over the other methods. First of all, the high sensitivity of a PZT patch directly bonded to a structure, together with a sophisticated electric impedance analyzer, demonstrates an excellent capability to map the dynamic properties of the structure. Second, because of the light weight and the low flexural stiffness of PZT patches, their attachment to a structure is essentially non-intrusive. The mass loading effect can be completely neglected in most of the practical cases and the limited stiffening effect may also be removed afterward by appropriate algorithms. Lastly, as an electrical quantity, the electric impedance is much easier to measure than a mechanical frequency response function and involves only one transduction device rather than the two involved in any other conventional method of structural FRF acquisition. This chapter will develop

a multi-input model of electromechanical interaction along with a measurement scheme, by which both point and transfer FRF in mechanical mobility can be acquired through electric impedance measurement.

2.2 Modeling of Electromechanical Interaction

2.2.1 Constitutive Formulation of Piezoelectric Effect

A piezoceramic material, most commonly known as PZT, short for Lead (Pb) Zirconate Titanate, exhibits a bi-directional "piezoelectric" effect. When the motion of the PZT in only one direction is considered and the stress, T, and the electric field, E, are chosen as the intensive variables, the electromechanical interaction between the stress, strain, electric field and flux density is governed by the following constitutive equations:

$$S_1 = s_{11}^E T_1 + d_{31} E_3 \tag{2.1}$$

$$D_3 = d_{31} T_1 + \varepsilon_{33}^T (1 - i\delta) E_3, \tag{2.2}$$

or, in the matrix form:

$$\begin{Bmatrix} S_1 \\ D_3 \end{Bmatrix} = \begin{bmatrix} s_{31}^E & d_{31} \\ d_{31} & \hat{\varepsilon}_{33}^T \end{bmatrix} \begin{Bmatrix} T_1 \\ E_3 \end{Bmatrix} \tag{2.3}$$

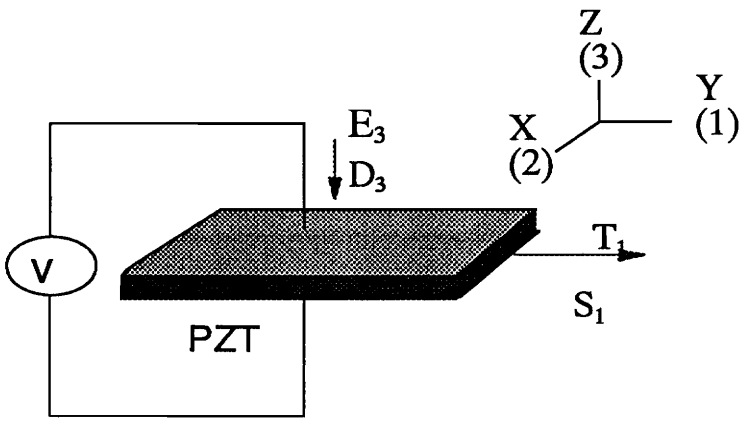

Figure 2.1 Electromechanical coupling of PZT.

where, as shown in Figure 2.1, S_1 is the strain and T_1 is the stress in the PZT along the y-axis; E_3 is the electrical field; and D_3 is the electric flux density along the z-axis between two parallel electrodes. s_{11}^E is the complex mechanical compliance at zero electric field; d_{31} is the piezoelectric constant at zero stress; ε_{33}^T is the dielectric constant at zero stress; and δ is the dielectric loss tangent of the PZT. The first equation is called the actuation equation and the second is the sensing equation. The two electrical quantities, the electric field E_3 and the flux density D_3 along the z-direction, are coupled with two mechanical quantities, stress T_1 and strain S_1, along the *y*-direction by the property matrix of the PZT. Here, the stress and the electric field are taken as intensive or independent variables; the mechanical strain and the electric displacement are independent variables.

2.2.2 Coupled Electric Admittance of Active PZT Sensors

When PZT actuators are embedded in a structure and activated by an ac field, the electromechanical interaction with the host structure can be formulated by a generic impedance model with multi-input, multi-output, as shown in Figure 2.2.

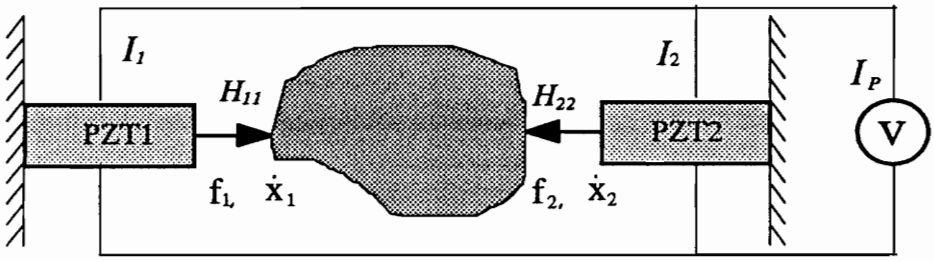

Figure 2.2 Multi-input, multi-output model of electromechanical interaction.

Two rod-type PZT actuators, with one end attached to a structure and the other end clamped, are driven by the same ac voltage source between their electrodes. Because of the induced strain, both PZTs tend to expand and contract along the direction perpendicular to the electric field applied. As the actuators are partially constrained by the structure, the reaction forces f_1 and f_2 are created. Meanwhile, velocity responses are developed at location 1 and 2 on the structure which can be expressed as:

$$\begin{Bmatrix} \dot{x}_1 \\ \dot{x}_2 \end{Bmatrix} = \begin{bmatrix} H_{11} & H_{12} \\ H_{21} & H_{22} \end{bmatrix} \begin{Bmatrix} f_1 \\ f_2 \end{Bmatrix}, \tag{2.4}$$

where H_{11} and H_{22} are the point mobility, and H_{12} and H_{21} are the transfer mobility of the structure. In a multi-input, multi-output system, the point mobility is defined as the velocity response developed by a unit force acting at the same point when all the other force inputs are zero. The transfer mobility is the velocity caused by the unit force acting on the other location while all the other force inputs are zero.

For each PZT actuator, the electromechanical interaction is governed by Equation 2.3. However, it is not in a convenient format, as the stress, strain, electric displacement and electric field are not readily measurable. Instead, the relationship between the electrical quantities and mechanical quantities can be formulated in terms of the electric current, voltage, force and velocity, which is standard for description of a two-port coupling transducer. As in this one dimensional model of the PZT interaction, the mechanical quantities are always in the *y*-direction and the electric quantities are always in the *z*-direction, we will drop all the subscripts in the later derivation.

The current flowing in PZT1 along the *z*-direction is the time rate of the total electric charge between the two electrodes and can be expressed as:

$$I_1 = \iint_{\sigma} i\omega D d\sigma \,, \tag{2.5}$$

where σ is the electrode area. For a rectangular PZT patch of width w, thickness h and length l, substitution of Equations (2.1) and (2.2) into (2.5) results in;

$$\begin{aligned} I_1 &= i\omega \frac{wl}{h}(\varepsilon - d^2 Y)V + wdYi\omega lS \\ &= i\omega \frac{wl}{h}(\varepsilon - d^2 Y)V + wdY\dot{x}_1 \end{aligned} \tag{2.6}$$

where $V = Eh$, Y is the elastic modulus of the PZT ($Y=1/s$), and the linear velocity of the PZT at its tip is the time derivative of the internal strain times the length $l\dot{x}_1 = i\omega lS$. Here, it is assumed that the standing wave along the PZT rod can be ignored. Substituting Equation (2.4) into (2.6), one gets:

$$I_1 = Y_c V + wdY(H_{11}f_1 + H_{12}f_2) \tag{2.7}$$

where

$$Y_c = i\omega \frac{wl}{h}(\varepsilon - d^2 Y). \tag{2.8}$$

The two terms in Equation 2.7 have clear physical meanings. The first term is the capacitive current which is solely determined by the material properties and the geometric dimensions of the PZT actuator and the energizing voltage. The second is the electromechanical interaction of the PZT with the structure. Y_c is the electric admittance of the PZT actuator when it is completely blocked, and it appears as a baseline in the coupled electric admittance, as shown in Fig. 3.5 (see next chapter). This can be proven by simply letting H_{11} and H_{12} equal zero in Equation 2.7, as an infinitesimal H_{11} means an infinite stiff structure.

The internal blocking stress of the PZT, T, may be obtained by letting strain $S=0$ in Equation (2.1), and the maximum output force (when the actuator has zero mechanical impedance) to the structure can then be determined by:

$$F_1 = -Twh = wdYV \tag{2.10}$$

Note that a minus sign is added to indicate that the output force is opposite to the internal stress. However, when the mechanical impedance of the PZT is considered, the force actually delivered to the structure by the PZT no longer equals the blocking force, but is a scale-down by the mechanical impedance of the structure and the actuator:

$$f_1 = \dot{x}_1 Z_{11} = F_1 \frac{Z_{11}}{Z_{11} + Z_{a1}}, \tag{2.11}$$

where Z_{11} and Z_{a1} are the mechanical impedance of the structure and the actuator, respectively. In the form of the mechanical mobility, it is:

$$f_1 = \frac{\dot{x}_1}{H_{11}} = F_1 \frac{H_{a1}}{H_{11} + H_{a1}}, \tag{2.12}$$

Similarly, the force the second PZT actuator delivers to the structure is:

$$f_2 = \frac{\dot{x}_2}{H_{22}} = F_2 \frac{H_{a2}}{H_{22} + H_{a2}}, \tag{2.13}$$

Assuming that the two PZT actuators are identical, then $H_{a1} = H_{a2} = H_a$. Substitution of Equations (2.10) - (2.13) into (2.7) yields the current expression in terms of structural mobility and energizing voltage:

$$I_1 = \{Y_c + (wdY)^2 (\frac{H_{11}H_a}{H_{11} + H_a} + \frac{H_{12}H_a}{H_{22} + H_a})\}V. \tag{2.14}$$

Similarly, the current for PZT2 is:

$$I_2 = \{Y_c + (wdY)^2(\frac{H_{21}H_a}{H_{11}+H_a} + \frac{H_{22}H_a}{H_{22}+H_a})\}V. \tag{2.15}$$

Using the superposition theory of linear system, the electric admittance of two PZT actuators connected in parallel can then be expressed as:

$$\begin{aligned} Y_p &= \frac{I_1 + I_2}{V} \\ &= 2Y_c + (wdY)^2(\frac{H_{11}H_a}{H_{11}+H_a} + \frac{H_{22}H_a}{H_{22}+H_a} + \frac{H_{21}H_a}{H_{11}+H_a} + \frac{H_{12}H_a}{H_{22}+H_a}) \end{aligned} \tag{2.16}$$

The electric admittance of a single PZT actuator can be determined by simply letting f_2 = 0 in Equation (2.7):

$$Y_{s1} = Y_c + (wdY)^2 \frac{H_{11}H_a}{H_{11}+H_a} \tag{2.17}$$

and similarly, the admittance of PZT2 alone is:

$$Y_{s2} = Y_c + (wdY)^2 \frac{H_{22}H_a}{H_{22}+H_a}. \tag{2.18}$$

Equation (2.16)-(2.18) list the three electrical quantities that are readily measurable by standard electric impedance analyzer. Both the single and parallel electric admittance have a similar format with the first term representing the capacitance characteristics of the PZT actuator and the second term representing the interaction with the structure through the piezoelectric coefficient *d*.

2.3 Extraction of Mechanical Mobility

The point mechanical mobility of a structure at location 1 can be derived from the electric admittance of a single PZT using Equations (2.17) and (2.18) as:

$$H_{11} = \frac{H'_{11} H_a}{H_a - H'_{11}} \tag{2.19}$$

where

$$H'_{11} = \frac{(Y_{s1} - Y_c)}{(wdY)^2}, \tag{2.20}$$

Similarly,

$$H_{22} = \frac{H'_{22} H_a}{H_a - H'_{22}}, \tag{2.21}$$

where

$$H'_{22} = \frac{(Y_{s2} - Y_c)}{(wdY)^2} \tag{2.22}$$

The transfer mobility between location 1 and 2 can be derived from Equation 2.16:

$$H_{12} = \frac{2H'_{12}}{H_a} \frac{(H_{11} + H_a)(H_{22} + H_a)}{(H_{11} + H_a) + (H_{22} + H_a)} \tag{2.23}$$

where

$$H'_{12} = \frac{Y_p - (Y_{s1} + Y_{s2})}{2(wdY)^2}. \qquad (2.24)$$

Equations (2.19) - (2.24) give the explicit expression of the structural mechanical mobility in terms of the measured electric admittance. Physically, Equation (2.19), (2.21) and (2.23) represent the structural mobility excluding the influence of the mechanical impedance of the PZT actuators while Equations (2.20), (2.22) and (2.24) are the approximation when the mechanical impedance of the actuator can be ignored. This may be seen in that when Ha approaches infinity, Equations (2.19), (2.21) and (2.23) converge to H'_{11}, H'_{22} and H'_{12}. Whether the mechanical impedance of the actuator can be neglected or not depends not only on the operating frequencies, but also on the location of the actuator with respect to the modal shape of the structure. For a particular PZT actuator with a certain free stroke, its mass is negligible if the operating frequency is far below the natural frequency of the actuator. Its stiffness is negligible if its free stroke is compatible with the motion of the structure at the location of attachment. This issue will be addressed more specifically in the later sections and the next chapter.

Although Equations (2.20), (2.22) and (2.24) are not necessary for the FRF extraction, they provide clear insight into the extraction process. For point mechanical mobility, it is the difference between the coupled admittance and the blocked admittance of a single PZT divided by a constant. The blocked admittance and the constant are solely determined by the material and the geometry of the PZT actuator. Similarly, the transfer mobility is

obtained by subtracting the electric admittance of each actuator when operated alone from the electric admittance of two PZTs when connected in parallel and then divided by the material constants. The exact solutions for mechanical mobility are obtained by manipulation of the approximate solution and the mobility of the actuators.

2.4 Surface-Bonded PZT Sensor-Actuator

2.4.1 Surface-Bonded PZT Actuation and Sensing

In typical applications of smart structures, the PZT actuators are embedded or integrated into a structure in the form of thin patches. There are many advantages to this type of attachment. First of all, an embedded PZT patch has a larger contact area with the structure, which will maximize its control authority as an actuator and its sensitivity as a sensor. Second, a bare and thin PZT patch is light and flexible so that its integration will have much less interference with the dynamics of the host structure than it would if the actuator is housed. Third, a bare PZT patch has a very simple structural dynamics at the frequency range of typical interests, the extraction of the structural FRF from the measured electric admittance of the actuator would be much easier. For these reasons, the bare and thin PZT patches are the most appropriate form of active sensor for structural dynamic measurement. This section will relate the impedance model developed above with the surface-bonded PZT actuation and sensing.

Although the multi-input model in Figure 2.2 implies that the actuators interact with the structure along the normal direction of the contact points, the results are also valid for the surface-bonded actuators which interact with structures through shearing of the adhesive layer.

The actuation mechanism of a surface-bonded actuator is somehow different from conventional shaker excitation. An electromagnetic shaker delivers to a structure a force normal to the surface, directly resulting in an out-of-plane motion. When a surface-bonded PZT patch expands or contracts along its longitudinal direction under an ac excitation, it shears the bonding layer, resulting a bending moment about the neutral layer of the structure which in turn yields a flexural vibration of the structure. However, for the PZT patch, it excites as well as senses the in-plane motion rather than the flexural motion. Thus, the point mobility and transfer mobility derived from the measured electric admittance of the PZT patches are "in-plane" properties of the structure, not the FRF in a conventional sense.

Figure 2.3 is a schematic diagram of the coupled electric impedance measurement. Two PZT patches are bonded to the surface of a structure at the locations at which structural mobility are to be measured. The electric admittance (the reciprocal of impedance) of each single PZT, Y_{S1}, Y_{S2} , and admittance of two PZTs in parallel, Y_P, are to be measured

respectively. It is important to note that $Y_P \neq Y_{S1}+Y_{S2}$ because of the mutual coupling. An additional admittance is created for each PZT due to the excitation from the other actuator. This additional admittance can be defined as the vibration-induced current in

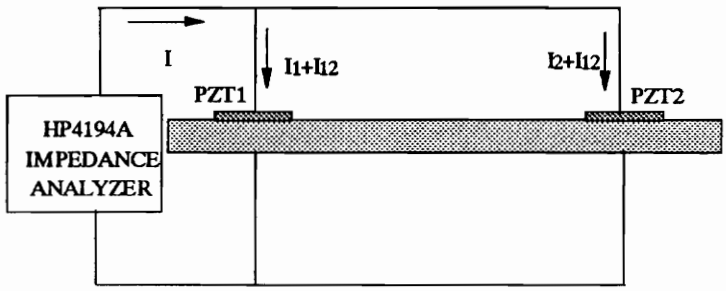

Figure 2.3 Measurement of the coupled electric impedance

PZT2 in short-circuit mode divided by the voltage across PZT1. It may not be measured directly, but can be deduced from the measurement scheme shown above. It is this coupled admittance that supplies information of the transfer mechanical FRF between location 1 and 2.

2.4.2 In-Plane Actuation — Pin-Force Model

As discussed in the previous section, the structural mobility obtained by the surface-bonded PZT actuators reflects the in-plane motions rather than the transverse deflection of the structure as the PZTs are bonded on the surface of the structure. Is this measurement scheme valid for the model developed above? The answer is positive if one looks at Figure 2.4. A surface-bonded PZT patch is an induced-strain device and can be considered as a

force source attached to the structure only at its two ends. The justification is that most of the shearing effect in the bonding layer, through which the actuator delivers excitation to the structure, is concentrated at the vicinity of its two ends. The actuation of the PZT on the structure can be represented by a pair of concentrated forces acting on two posts at the ends of actuator. This is well known as the "pin-force model" of PZT actuation (Bailey and Hubbard, 1985; Crawley and Andson, 1990), or the "enhanced pin-force model"

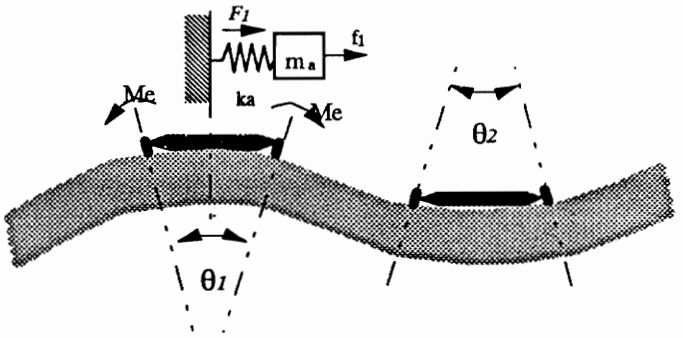

Figure 2.4 Pin-force model of in-plane actuation.

(Chaudhry and Rogers, 1991), and is widely used in solid state actuation modeling. Furthermore, because of the symmetric actuation, the center of the PZT is always still. Thus, the actuator can be modeled as a mass-spring oscillator with one end clamped and the other end acting on the structure. The SDOF system has an equivalent mass of approximately 1/6 of the mass of the PZT and an equivalent stiffness of twice as the PZT's longitudinal stiffness. Clearly, this model of the in-plane actuation allows for the use of Equation (2.19), (2.21) and (2.23).

Figure 2.4 also shows another advantage of sensing and actuation using surface-bonded PZT patch: elimination of the need for support of the actuator, either by the inertia of the actuator or by fixing it to ground, as required by any out-of-plane motion excitation devices.

It is worth mentioning that any transducer which has a bi-directional transduction effect is theoretically qualified for structural signature acquisition through its electric impedance measurement. For instance, the electric impedance of an electromagnetic shaker while driving a structure also contains information about the structural signature. The same is true for a PZT stack actuator. However, the massive and stiff housing of an electromagnetic shaker can substantially reduce the sensing capability and result in a significant change in the dynamics of the structure. In addition, the extraction of the structural signature will become more difficult and less reliable than with simple PZT patches because of its more complicated structural dynamics.

2.4.3 Relation Between In-Plane Mobility And Rotational Mobility

Figure 2.4 also reveals another important relation between the in-plane linear motion of the actuator and the structural rotational mobility, which is defined as the angular velocity difference divided by the bending moment. For instance, the point rotational mobility of the structure at location 1 is defined as:

$$H_{R11} = \frac{\dot{\theta}_1}{M_e} = \frac{\theta_1}{M_e}\omega i, \tag{2.25}$$

and, similarly, the transfer rotational mobility between location 1 and 2 is:

$$H_{R22} = \frac{\dot{\theta}_2}{M_e} = \frac{\theta_2}{M_e}\omega i, \tag{2.26}$$

The point rotational mobility is related to the in-plane linear mobility of the structure by:

$$H_{R11} = \frac{H_{11}}{(h_p/2 + h_s/2)^2}, \tag{2.27}$$

and similarly, the transfer rotational mobility is:

$$H_{R12} = \frac{H_{12}}{(h_p/2 + h_s/2)^2}, \tag{2.28}$$

where h_P and h_S are the thickness of the PZT and the distance from the surface to the neutral plane of the structure, respectively. While the rotational structural mobility measurement has been a challenge with most conventional vibration transducers, the surface-bonded measurement method offers an easy solution.

2.4.4 Impact of Actuator Length on Extracted Mobility

Figure 2.4 and Equations (2.24) - (2.28) imply an important fact that the in-plane structural mobility as well as the rotational mobility are functions of the distance between two imaginary posts. The mobility, thus obtained, reflects the average deflection

curvature of this segment of the structure. Generally, the longer the actuator, the higher the mobility. However, this is not always the case, as a PZT patch is a distributed sensor. Its electric admittance reflects the overall vibration response over its area. As the curvature may change sign within the length of the actuator, the electric admittance is a complicated function of the area and the location of the actuator, as well as the modal shape of the structure. The electric admittance of an active PZT sensor can take the form of:

$$Y_{s1} = \frac{i\omega wl}{h}\varepsilon_{33}(1-i\delta) + \frac{i\omega}{V}\iint_{\sigma} d_{31}T dxdy. \tag{2.29}$$

For a one-dimensional structure, for instance, a beam, the surface stress is:

$$T = -Y(\frac{h_s + h_a}{2}\kappa(x) - d_{31}E), \tag{2.30}$$

where $\kappa(x)$ is the curvature of the structure at location x and h_s is the thickness of the structure. Equation (2.29) may then be expressed as:

$$Y_{s1} = Y_c - \frac{i\omega wYd_{31}(h_s + h_a)}{2V}\int_{x_s}^{x_s+l_a}\kappa(x)dx. \tag{2.31}$$

It is clear that, unless the curvature of the structure is a constant, a PZT patch sensor with finite length always averages out the interaction term through the integration and results in an electric admittance, Y_{s1}, biased either lower or higher than it would be if the length were zero. Therefore, a shorter PZT is preferable for the accuracy of the mobility, especially when high-order vibration modes are to be involved whose spatial wavelength may be comparable to the length of the sensor. However, a short PZT sensor will

certainly reduce its sensitivity and signal-to-noise ratio, and result in less reliable results. In practice, the length of the PZT sensor should be smaller than the wavelength of the highest mode of the structure to be considered.

2.5 Case Study: Mobility Extraction of a Free-Free Beam

2.5.1 Test Instrumentation and Results

A proof-of-concept test was conducted on a small aluminum beam of 95.24×21.12×1.54

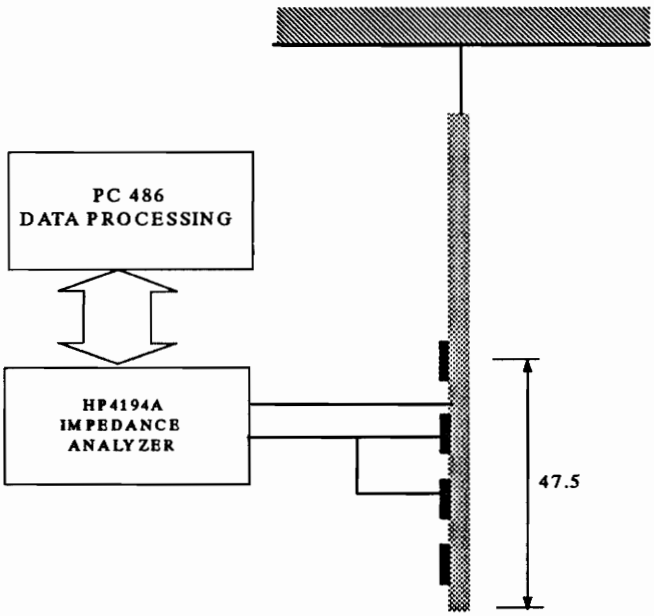

Figure 2.5 Measurement set-up

mm. The beam is slender and flexible so that attachment of any conventional excitor and

transducer will obviously result in questionable data. Four tiny PZT patches were bonded to the beam with uniform spacing in-between by Loctite Super Bond 495. The beam was suspended in air by a very thin fishing line, as shown in Figure 2.5. To minimize the introduction of external damping to the beam, all the electrical connections were by single-shred wires of 0.1 mm. The electric admittance of each individual PZT and each PZT pair were measured separately.

The equipment used to measure the electric admittance is an HP4194A impedance/phase-gain analyzer manufactured by Hewlett-Packard. This analyzer is designed for the measurement of electric and electronic components as well as other electric network under a weak electric field. The measurement functions include electric impedance, admittance, equivalent circuit, et al. It has a maximal oscillation output voltage level of 2.8 V_{p-p}. A complex Weston Bridge unit measures the current flowing in the device under test. The electric impedance is then digitally calculated and displayed in either Bode plot or real-and-imaginary format. The start frequency, stop frequency and the frequency interval are user-selectable. Up to 401 data points are available in the selected frequency range. The analyzer also provides an option of dc bias up to 40 volts to facilitate the needs of some nonlinear devices. The extremely high sensitivity and repeatability makes this machine ideal for the implementation of this electromechanical technique. The analyzer is connected to a personal computer 486DX by an HPIB interface card through which the measured data is transferred to the computer for further processing. The analyzer can be

set up in the PC through the HPIB bus. The whole process of measurement and extraction can be automated by a program written in QBASIC running on the PC.

For this particular beam, a sweeping frequency range from 100 Hz to 3500 Hz is selected which covers its first 7 flexural vibration modes. Both point and transfer mobility are then extracted using Equations (2.19) - (2.24). Table 2.1 gives the material constants of the PZT and their geometric dimensions used for extraction. The results are given in magnitude and phase, and are listed in the Appendix A.

Table 2.1 Material constants and geometry of the PZT sensors

d_{31}	Y	ε_{33}^{T} *	δ *	w	l	h
m/v	N/m^2	F/m		mm	mm	mm
-166e-12	6.30e10	1.50e-8	0.02	8.3	10.2	0.19

The validity of the data can be quickly checked against some well-known fundamental features of structural mechanical mobility. First, the point mobility H_{11} through H_{33} all show that an antiresonance always precedes a resonance peak. The only exception is the absence of the second antiresonance of H_{22}. The explanation for this irregularity is the dynamic range limitation (especially at the low frequency end) of the HP4194A impedance analyzer, which has only $1V_{rms}$ oscillation level and 12 bit A/D converter. For the transfer mobility H_{12}, H_{23}, H_{34} and H_{24}, they do not follow this pattern but have the antiresonances and the minimums interwoven irregularly, depending on the location. These are the key characteristics of the mechanical mobility of a free-free (non-grounding) system. Second,

the phases for all the point mobility are essentially either $\pi/2$ or $-\pi/2$ at off-resonance frequencies. There is always a zero-crossing of the phase at each resonance and no phase change at any antiresonance frequencies. However, the detailed verification of the data needs to be conducted by either sophisticated transducers or analytical simulation.

2.5.2 Residual Stiffening Effect of PZT Sensor-Actuators

The surface-bonded PZT minimizes the effect of mass loading and stiffening of the actuators on a structure. However, this does not necessarily mean there is no need for correction for the residual stiffening. In some cases, this stiffening can still be noticeable and the use of the approximate version of the mobility extraction should be avoided.

In Figure 2.6, the extracted point mobility H_{22} is plotted along with its approximation version H'_{22} for comparison. The dotted line is the mechanical mobility of the PZT actuator,

$$H_a = -j\frac{\omega}{m_a\omega^2 - k_a}, \tag{2.32}$$

which is modeled as an SDOF oscillator to take care of both the mass load and stiffening. Apparently, for the frequency band selected and the size of the PZT actuator used in this beam test, the stiffness is overwhelmingly dominant, as indicated by a clear stiffness line across the whole band (dotted line). The severity of the stiffening for each vibration mode

varies drastically, depending on the extent of mobility matching. As can be seen, modes 6 and 7 have higher mobility than the PZT; in other words, the PZT constitutes a constraint to the motion of the beam under these frequencies. As a result, the natural frequencies are significantly shifted up (25 Hz for the 7th mode and 11 Hz for 6th mode). Meanwhile, the point mobility is much lower than that of the PZT for modes 1, 4 and 5. Consequently, these modes are not stiffened by the PZT at all. For modes 2 and 3, the mobility are nearly compatible so there is also no stiffening. Figure 2.6 provides a quick check for the need for stiffening correction in the extraction process. Only those modes whose extracted mobility is much higher than that of the actuator will need correction for natural frequencies.

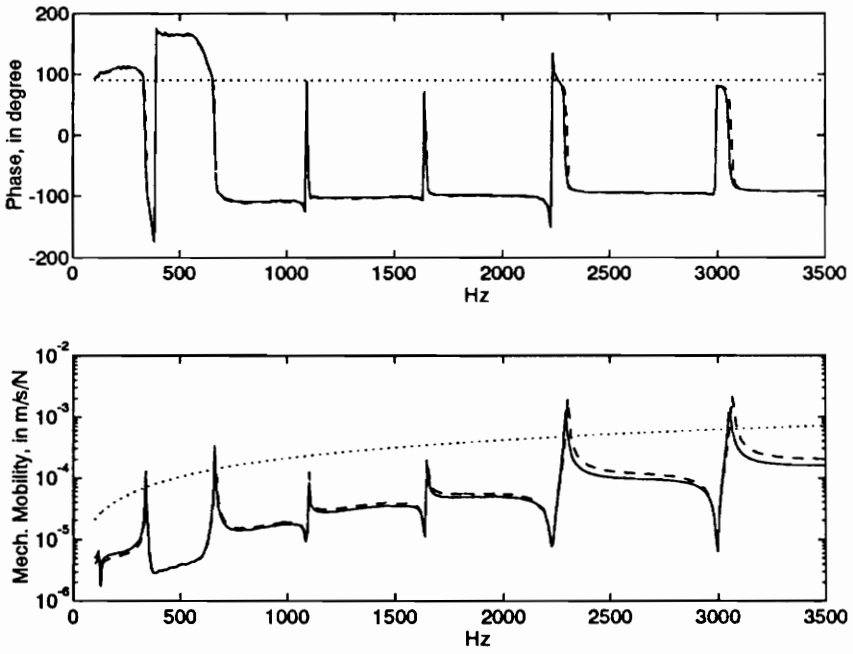

Figure 2.6 Residual stiffening effect of PZT actuators (— H22, --- H22', ...Ha).

2.5.3. Sensitivity of Mobility to Bonding Layer

The fidelity of the extracted mobility relies not only on the accuracy of the electric admittance but also on certain material and geometric constants of the PZT actuator used to extract the FRF. As can be seen from the derivation of the mobility expression, the process of the extraction is essentially to "strip off" the capacitive component, or the base line of the electric admittance (electric admittance of a blocked PZT actuator, Y_c) and to retain the interaction part. Of the parameters listed in Table 2.1, the dielectric constant and the thickness of the PZT are found to have the most significant impact on the quality of the results. A small deviation of the dielectric constant or the thickness will lead to a significant distortion in the FRF. There is an uncertainty in determining the true values of these two parameters in practice. The PZT is usually directly bonded to the structure by an adhesive to ensure a maximal mechanical interaction. The surface of the structure serves as one of the electrodes to provide the electric field to the piezoceramic patch, as shown in Figure 2.7. The cured non-conductive adhesive layer then constitutes a part of the capacitor. Consequently, the equivalent dielectric constant and the equivalent thickness that the impedance analyzer "sees" may significantly deviate from its nominal values, which will be used for extraction. Furthermore, the thickness of the adhesive layer varies with each PZT, depending on the viscosity and the pressure applied during its curing. Although the problem can be solved by taking the electric connection directly off the bottom silver electrode, it involves use of a thin copper foil between the PZT patch

and the structure. This will compromise the interaction of the PZT with the structure and result in a weaker excitation and sensing. Care must be given to the bonding process to ensure an adhesive layer as uniform and thin as possible. Very often, a minor adjustment of the equivalent thickness and dielectric constant will be required to reduce obvious distortion in the baseline of the extracted FRF.

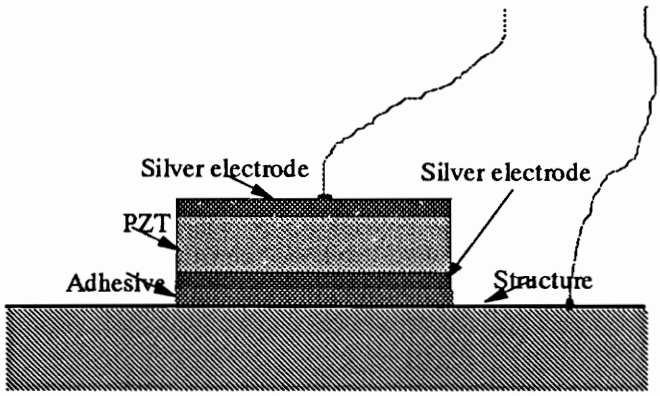

Figure 2.7 Adhesive layer and its effect

Summary

The structural mobility extraction through electric impedance measurement provides an alternative to the conventional frequency response function acquisition. With the measurement of electric impedance, the instrumentation and transduction is greatly simplified. The use of a surface-bonded PZT patch as an active sensor reduces the transducer mass loading and stiffening to a minimum level. The technique of coupled

electric impedance measurement in conjunction with the multi-input interaction modeling allows for a complete extraction of both point mobility and transfer mobility. The model can also eliminate the residual stiffening effect when needed. These features make the method ideal for structural dynamic analysis of small and flexible structures that are extremely sensitive to the attachment of transducers.

Chapter 3

Structural Modal Analysis by Surface-Bonded PZT Sensor-Actuators

This chapter presents a structural modal analysis technique based on the electric admittance measurement of surface-bonded active sensors. The model governing the electromechanical interaction of bonded PZT sensor-actuators with host structures developed in the previous chapter is modified to accommodate the extraction of modal parameters from the measured electrical admittance. The work focuses on the uniqueness of this electromechanical approach for modal parameter extraction. Two corresponding modal parameter extraction algorithms are presented. Both exclude the stiffening effect of the PZT on the structure, yielding better estimations of natural frequencies and modal damping.

3.1 Introduction

Experimental modal testing has now become a mature and standard technique in structural dynamic analysis. It usually consists of several independent steps: structure excitation, measurement of driving force and vibration response, formation of Frequency Response

Function (FRF), and modal parameter extraction. The entire process requires a set of sophisticated pieces of equipment, such as a multi-channel signal analyzer, force and response transducers, shakers, power amplifiers, and various types of signal conditioners. The typical transducers used in a modal testing are piezoceramic force gauges, accelerometers and electromagnetic shakers. The attachment of conventional transducers onto structures may result in considerable errors in the extracted modal parameters, especially when dealing with light and flexible structures. The use of a Laser Doppler Vibrometer or an eddy current sensor provide a non-contact measurement of structural response, but an attachment of the force gauge and shaker to the structure is still needed. In engineering practice, many application requires that the structural dynamic measurement be conducted non-intrusively. As discussed in the last chapter, the surface-bonded PZT patch as an active sensor, along with an electric impedance analyzer, appears to provide an excellent solution to this challenge.

This chapter presents a technique of structural modal testing using a surface-bonded piezoceramic patch and electric impedance measurement. The mechanical mobility extracted by the multi-input model can be directly used for structural modal analysis by various conventional approaches that are not to be addressed here. The emphasis of this work will be on the uniqueness of the modal parameter extraction using the electric impedance approach. The model governing the electromechanical interaction of the actuator and the structure is derived in a slightly different way to accommodate the direct

modal parameter extraction. Two algorithms of modal parameter extraction associated with the technique are developed. One uses electric admittance match/half-power band-width method, and the other employs revised Nyquist plane curve fitting. Both algorithms can extract the modal damping coefficients, natural frequencies and curvature mode shapes of a structure. The model has considered the stiffening effect of the actuator on the structure, yielding refined estimations of extracted structure natural frequencies. This is critically important when the test piece is flexible and small.

3.2 Electromechanical Model

For modal parameter extraction, the model in Figure 2.2 is modified to include the modal mass, modal stiffness and modal damping of the structure. Also, for the simplicity of the

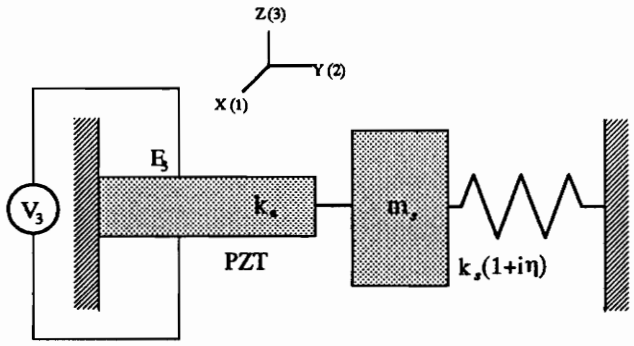

Figure 3.1 SDOF model of electromechanical interaction of a PZT with a structure.

modeling, only single input is used, as shown in Figure 3.1.

Using the same derivation as in the previous chapter, we obtain the expression of the current flowing in the PZT actuator in terms of the mechanical impedance of the structure and the actuator:

$$I = i\omega \frac{wl}{h}[\varepsilon_{33}^{T}(1 - i\delta) - \frac{Z_s}{Z_s + Z_a}(d_{31})^2 Y]V, \tag{3.1}$$

where Z_s is the mechanical impedance of the structure, and Z_a is the mechanical impedance of the actuator along its length. The coupled electric admittance of the PZT then becomes:

$$Y_e = \frac{I}{V} = i\omega a[\varepsilon_{33}^{T}(1 - i\delta) - \frac{Z_s}{Z_s + Z_a}(d_{31})^2 Y] \tag{3.2}$$

where $a = \frac{w\ l}{h}$. Note that a uniform distribution of electric flux density in the PZT is assumed in the integration. Similar to Equation (2.7), the first term in Equation (3.2) is the capacitance admittance and the second term is the result of the electromechanical interaction of the PZT with the structure.

3.3 Modal Parameter Extraction

To demonstrate the application of this electromechanical approach for modal analysis, a single-degree-of-freedom (SDOF) model for extraction is developed. The mechanical impedance of the PZT element in Figure 3.1 may be expressed as:

$$Z_a = -\frac{i}{\omega} k_a, \tag{3.3}$$

where k_a is the short-circuit stiffness of the PZT along the y-axis. The effect of the PZT's mass along the *y*-direction is neglected, assuming that the stress wavelength is much larger than the PZT's characteristic dimension under normal operating frequency. The mechanical impedance of an SDOF system with structure damping is given by (Ewins, 1984):

$$Z_s = i(m_s\omega - \frac{k_s(1+i\eta)}{\omega}), \tag{3.4}$$

where m_s is the modal mass, k_s the modal stiffness and η the modal damping. Substituting Equations (3.3) and (3.4) into Equation (3.2) yields the electric admittance of the actuator in terms of the modal parameters of the structure:

$$\begin{aligned} Y_e = \omega a[\varepsilon\delta + \frac{ck_a k_s \eta}{(k_s\eta)^2 + (k_s + k_a - m_s\omega^2)^2} \\ +i(\varepsilon - c + \frac{ck_a(k_s + k_a - m_s\omega^2)}{(k_s\eta)^2 + (k_s + k_a - m_s\omega^2)^2})] \end{aligned}, \tag{3.5}$$

where $c = (d_{31})^2 Y$. Separation of the real and imaginary parts of Equation (3.5) results in the expression:

$$H_r = (\frac{\mathrm{Re}(Y_e)}{\omega a} - \varepsilon\delta)/c = \frac{k_a k_s \eta}{(k_s\eta)^2 + (k_s + k_a - m_s\omega^2)^2} \tag{3.6}$$

$$H_i = (\frac{\mathrm{Im}(Y_e)}{\omega a} - \varepsilon - c)/c = \frac{k_a(k_s + k_a - m_s\omega^2)}{(k_s\eta)^2 + (k_s + k_a - m_s\omega^2)^2}. \tag{3.7}$$

As a PZT actuator usually has a size much smaller than that of the structure, its mechanical damping can be ignored. Equations (3.6) and (3.7) trace out a non-closing circle in a Nyquist plane as shown by Equation (3.8):

$$(H_r - \frac{k_a}{2k_s\eta})^2 + H_i^2 = (\frac{k_a}{2k_s\eta})^2, \tag{3.8}$$

This is the locus of the mechanical mobility of a SDOF system with proportional damping connected in parallel with a massless spring, K_a (Ewins, 1984).

3.3.1 Revised Nyquist Plane Curve Fitting

Equations (3.6) and (3.7) are highly nonlinear functions of the modal parameters. It is much easier to conduct the curve fitting to the impedance plot in the Nyquist plane than to extract modal parameters from the mobility. The mechanical impedance of SDOF with structural damping takes the simple form (Ewins, 1984):

$$Z = \frac{1}{H_r + iH_i} = \frac{k_s}{k_a}\eta - i\frac{k_s + k_a - m_s\omega^2}{k_a} \tag{3.9}$$

The mechanical impedance traces out a straight line on the inverse Nyquist plane, as shown in Fig. 3.2. Note that due to the stiffening effect of the PZT on the structure, the intersection of the line with the real axis no longer defines the natural frequency of the SDOF system alone but, rather defines the natural frequency of the PZT-SODF joint structure. Curve fitting the measurement data to the imaginary part of Equation (3.9) yields two quantities, k_S/k_a and $m_S//k_a$. Note that they are the structural modal stiffness

and modal mass normalized to the actuator modal stiffness, and none of them has a physical meaning. However, the natural frequency of the structure can be determined from them as:

$$\omega_r = \sqrt{k_s / m_s} = \sqrt{(k_s / k_a)/(m_s / k_a)}, \tag{3.10}$$

Another independent curve fitting the measurement data to the real part of the equation yields a refined estimation of Re(Z), and from it the structural modal damping can be calculated as:

$$\eta = \frac{\mathrm{Re}(Z)}{k_s / k_a} \tag{3.11}$$

Equations (3.9), (3.10) and (3.11) constitute the revised Nyquist Plane Curve Fitting approach, which will be referred to as NPCF later. The difference with the standard Nyquist plane curve fitting approach is the inclusion of the actuator stiffness.

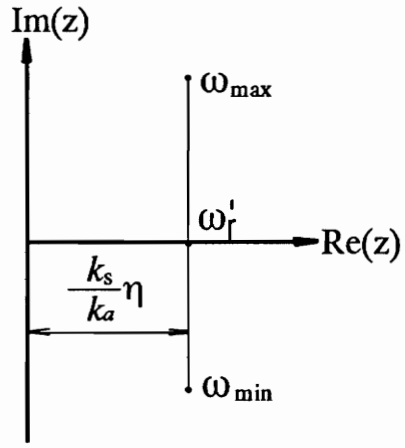

Figure 3.2 Mechanical Impedance of SDOF in inverse Nyquist plane

3.3.2 Admittance Matching/Half Power Bandwidth

Equations (3.6) and (3.7) together provide a new approach to the determination of the modal damping η and natural frequency ω_r of a structure. Take the partial derivative of Equation (3.7) with respect to ω and let it be zero:

$$\frac{\partial(H_i)}{\partial\omega} = \frac{-2k_a m_s[(k_s\eta)^2 - (k_s + k_a - m_s\omega^2)]}{[(k_s\eta)^2 + (k_s + k_a - m_s\omega^2)^2]^2} = 0. \tag{3.12}$$

This yields two solutions:

$$k_s\eta = (k_s + k_a - m_s\omega_1^2) \tag{3.13}$$

$$k_s\eta = -(k_s + k_a - m_s\omega_2^2) \tag{3.14}$$

where ω_1 and ω_2 correspond to the peak and valley of H_i, respectively. Addition of Equations (3.13) and (3.14) yields structural modal damping in terms of special frequencies:

$$\eta = \frac{1}{2\omega_r^2}(\omega_2^2 - \omega_1^2), \tag{3.15}$$

where

$$\begin{aligned} \omega_r^2 &= k_s / m_s \\ \omega_1^2 &= (k_s(1-\eta) + k_a)m_s \\ \omega_2^2 &= (k_s(1+\eta) + k_a)m_s, \end{aligned} \tag{3.16}$$

The natural frequency of the structure, ω_r, can be determined by the special points of the coupled electric admittance, Y_e. At resonance of the structure, the mechanical impedance,

Z_s, diminishes and Equation (3.2) is deduced to the electric admittance of the "free" PZT actuator.

$$Y_{ef} = \omega a \varepsilon_{33}^{T} (\delta + i) \tag{3.17}$$

Similarly, the electric admittance of a blocked PZT actuator can be obtained by letting Z_S be ∞. This yields:

$$Y_{eb} = \omega a \, (\varepsilon_{33}^{T}\delta + i(\varepsilon_{33}^{T} - c)) . \tag{3.18}$$

The imaginary parts of both admittance $\mathrm{Im}(Y_{ef})$ and $\mathrm{Im}(Y_{eb})$ intersect with the imaginary part of the coupled admittance $\mathrm{Im}(Y_e)$, as is illustrated in Figure 3.3. It is apparent by definition that it is the intersection of $\mathrm{Im}(Y_{ef})$ with $\mathrm{Im}(Y_e)$ that determines the natural frequency of the structure ω_r (impedance matching). By checking Equation (3.9), it is not difficult to see that the intersection of $\mathrm{Im}(Y_{eb})$ with $\mathrm{Im}(Y_e)$ corresponds to the natural frequency of the joint system of the PZT and the SDOF system:

$$\omega_r' = \sqrt{\frac{k_s + k_a}{m_s}}, \tag{3.19}$$

at which $\mathrm{Re}(Y_e)$ peaks and the interaction portion of $\mathrm{Im}(Y_e)$ vanishes. The difference between the two frequencies is, once again, caused by the stiffening of the PZT sensor. Note that in Equation (3.16), ω_r is the characteristic of the structure alone ,and ω_1 and ω_2 are those of the joint system. This distinguishes it from the conventional half-power band width method, by which the damping is calculated by ω_1, ω_2 and ω_r'. It will be referred to as the admittance matching / half-power band-width (AM/HPB) approach later.

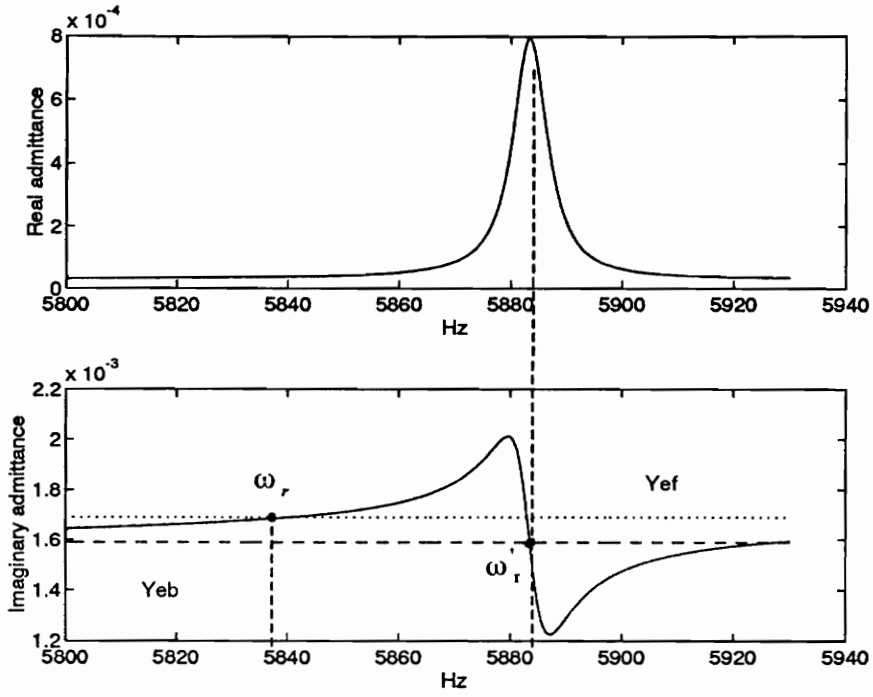

Figure 3.3 Determination of structural natural frequency by electric admittance matching.

3.3.3 Modal Shapes Extraction

Equations (3.6) and (3.7) also provide a way of eigenvector extraction when applied to a multi-degree-of-freedom system or continuum system. At the system resonance ω_r', $H_i = 0$ and

$$H_r = \frac{k_a}{k_s \eta} = \frac{k_a}{\eta} y \tag{3.20}$$

where y is the modal displacement response to a unit force excitation ($y = 1/k_s$). For a continuum structure, this modal displacement is a function of measurement coordinate and vibration mode. The modal stiffness of the PZT, k_a and the structural modal damping, η,

vibration mode. The modal stiffness of the PZT, k_a and the structural modal damping, η, for a particular mode is independent of the coordinate. When H_r is extracted at m coordinates along the structure for each of its n modes, the eigenvector can be obtained and its element takes the form :

$$H_r(i,j) = \frac{k_a(i)}{\eta(i)} y(i,j), \tag{3.21}$$

where i = 1,2,...n and j = 1,2...m. This can also be directly deduced from the fact that $k_a / k_s \eta$ is the diameter of the modal circle in the Nyquist plane.

3.4 Case Study: Modal Testing of a Free-Free Beam

3.4.1 Test Set-up And Procedures

System identification of a small and flexible structure is usually a challenge as the extracted structural modal parameters are extremely sensitive to the stiffening and mass loading of the attachment of sensors and actuators. By using surface-bonded PZT sensor-actuators, these effects can be minimized. As an example, a proof-of-concept test was conducted on an aluminum beam of 153.0×25.7×0.8 mm. A PZT patch of 32×19×0.19 mm is bonded on the beam 52 mm from the end of the beam. The size of the PZT is considerable compared with that of the beam, so that its stiffening effect to the beam can be fully demonstrated and the performance of the proposed algorithms can be thoroughly

investigated. The beam is suspended in air by very thin wires to simulate a free-free boundary condition and to minimize the possibility of introducing external damping. The electric impedance of the PZT patch is measured over a broad frequency band by the HP 4194A Impedance Analyzer. Figure 3.4 is the schematic diagram of the experimental set-up.

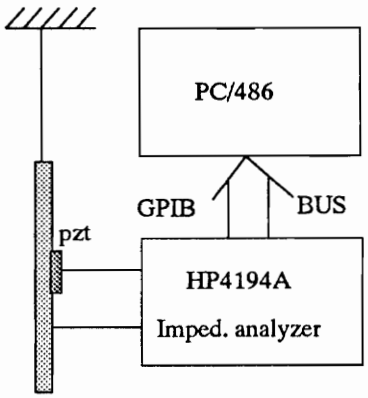

Figure 3.4 Experimental set-up of the beam modal analysis.

Figure 3.5 is the electric admittance of the PZT patch from 100 Hz to 7000 Hz, in which the first 9 flexural vibration modes of the beam are clearly identifiable. Note that each mode is well separated from the others. This qualifies the application of the SDOF model to the data. For the actual parameter extraction, each mode is zoomed in to obtain a much higher frequency resolution and amplitude accuracy.

To obtain the uncontaminated natural frequencies of the beam, the original PZT patch is then replaced by a tiny one (4×6×0.19 mm) and its admittance is measured. It is assumed

that the stiffening of this tiny PZT is negligible as its length is less than 1/6 of the original one. Therefore, the resonant peaks of its admittance may well represent the "true" natural frequencies of the beam.

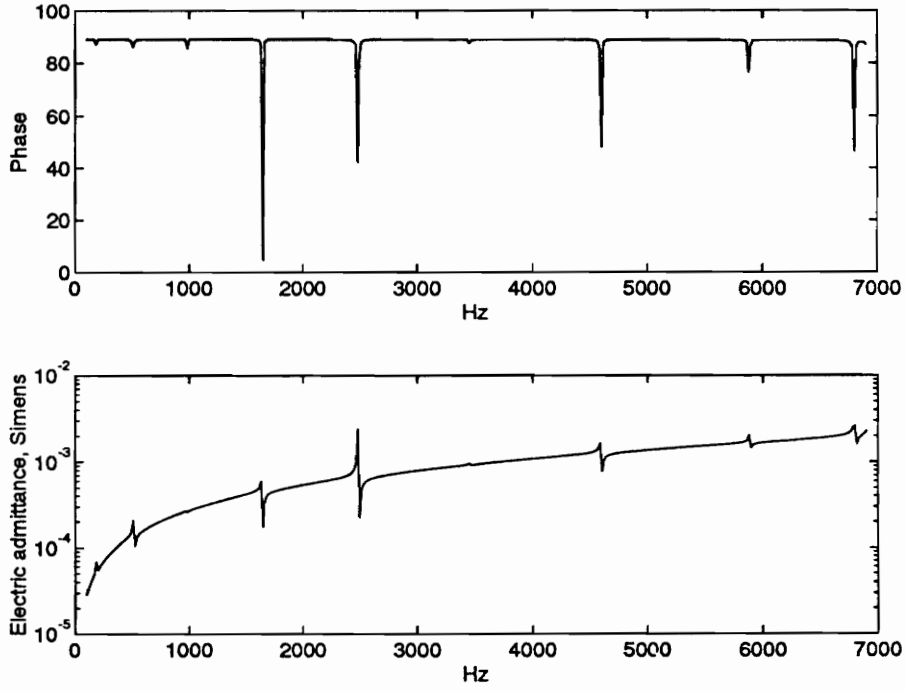

Figure 3.5 Coupled electric admittance of a PZT bonded to a beam.

3.4.2 Test Results

Table 3.1 shows the natural frequencies and modal damping of the beam extracted respectively by the two algorithms previously discussed. Table 3.2 lists the natural

frequencies of the beam versus the estimations by the electric admittance of the large PZT sensor.

Table 3.1 Extracted natural frequencies and modal damping of a free-free beam

Mode	1	2	3 *	4	5	6 *	7	8
f_{r1}(Hz)	185.9	498.3	982.0	1628.4	2437.5	3457.6	4588.5	5893.8
η_1 (%)	0.37	0.37	0.15	0.20	0.22	0.13	0.16	0.17
f_{r2}(Hz)	187.6	497.2	982.2	1628.0	2439.9	3456.0	4588.2	5891.7
η_2 (%)	0.21	0.31	0.095	0.15	0.18	0.064	0.15	0.17

Subscript 1: AM/HPB

Subscript 2: NPCF

Table 3.2 Error estimation of natural frequencies without correction for stiffening

Mode	1	2	3 *	4	5	6 *	7	8
f_{rj} (Hz)	189.3	516.7	983.0	1656.8	2493.1	3459.9	4622.5	5913.3
f_{rs}(Hz)	183.3	494.7	982.5	1621.8	2437.5	3455.2	4580.6	5863.4
E_{js} (%)	+3.2	+4.4	+0.05	+2.2	+2.3	+0.14	+0.9	+0.85

f_{rj}: natural frequencies of PZT-beam joint structure

f_{rs}: natural frequencies of the beam

$E_{js} = (f_{rj} - f_{rs}) / f_{rs}$, $E_{js\ max.} = 4.4$ % and $E_{js\ average} = 1.62$ %.

To verify the algorithms' capability of correcting the natural frequencies for stiffening effect, the relative errors of the corrected natural frequencies with respect to the beam natural frequencies are calculated and listed in Table 3.3.

Table 3.3 Error estimation of extracted natural frequencies

Mode	1	2	3 *	4	5	6 *	7	8
E_1(%)	+1.40	+0.67	-0.05	+0.33	0	+0.07	+0.17	+0.51
E_2(%)	+2.30	+0.51	+0.03	+0.38	+0.10	+0.02	+0.17	+0.48

$E_1 = (f_{r1} - f_{ns}) / f_{ns}$, $E_{1max} = +1.40$ % and $E_{1average} = 0.41$ %

$E_2 = (f_{r2} - f_{ns}) / f_{ns}$, $E_{2max} = +2.30$ % and $E_{2average} = 0.49$ %

Table 3.4 lists the material constants of the PZT sensor used.

Table 3.4 Material constants of the PZT sensor

d_{31}, m/v	Y, N/m^2	ε_{33}^T F/m	δ *
-166e-12	6.30e10	1.50e-8	0.02

3.4.3. Result Analysis

Although the electric admittance of the PZT gives approximate estimations of the natural frequencies of the beam, they are consistently biased higher than the "true values", as illustrated in Table 3.2. This bias can be up to 4.4% with an average of 1.62% for the first 8 flexural modes. Obviously, the stiffening, rather than the mass loading, of the PZT on the beam dominates within this frequency range. This stiffening generally introduces more impact on low modes than high modes in terms of the relative shift in natural frequencies. This demonstrates the need of correction for the stiffening effect when using surface-bonded PZT for precision modal testing of structures.

Table 3.3 lists the relative errors of the corrected natural frequencies with respect to the true natural frequencies of the beam. Note that the maximum errors reduce to 1.4% and 2.3% at the first mode, and average errors reduce to 0.41 % and 0.49 %, respectively. Although the results from the two algorithms vary slightly, both of them produce better estimations of the true values of the natural frequencies in the sense that average error decreases by 75%.

The demand for the frequency correction varies with each mode for this particular PZT location. As one can see in Fig. 3.5, the strength of each mode varies significantly. Figure 3.6 (a)-(b) show the imaginary parts of the admittance of the PZT when it is fully coupled, free and blocked, which demonstrates four typical cases of the stiffening levels. For mode 1 and mode 2 (Figure 3.6a and 3.6b), Im(Y_{cf}) intersects with Im(Y_c) before the resonance of the stiffened structure, which implies that the in-plane vibration of the beam is stronger than the free stroke of the PZT actuator. In other words, the PZT actuator is constraining the beam, and substantial stiffening occurs. For mode 3 (Figure 3.6c), the two motions are completely compatible, neither of them imposes constraint on the other. This is indicated by the tangency of the two curves. As for Figure 3.9(d), mode 6 is marginally activated. The motion of the PZT for this particular mode is nearly being blocked by the beam, or in other words, the PZT is "stiffened" by the beam rather than vice-versa.

This variation of the stiffening with modes can also be seen from Table 3.2 that the relative frequency deviation for mode 3 and mode 6 are much smaller than for the other modes. Obviously, there is little need for frequency correction for these two modes. Therefore, the application of frequency correction algorithms should be selective.

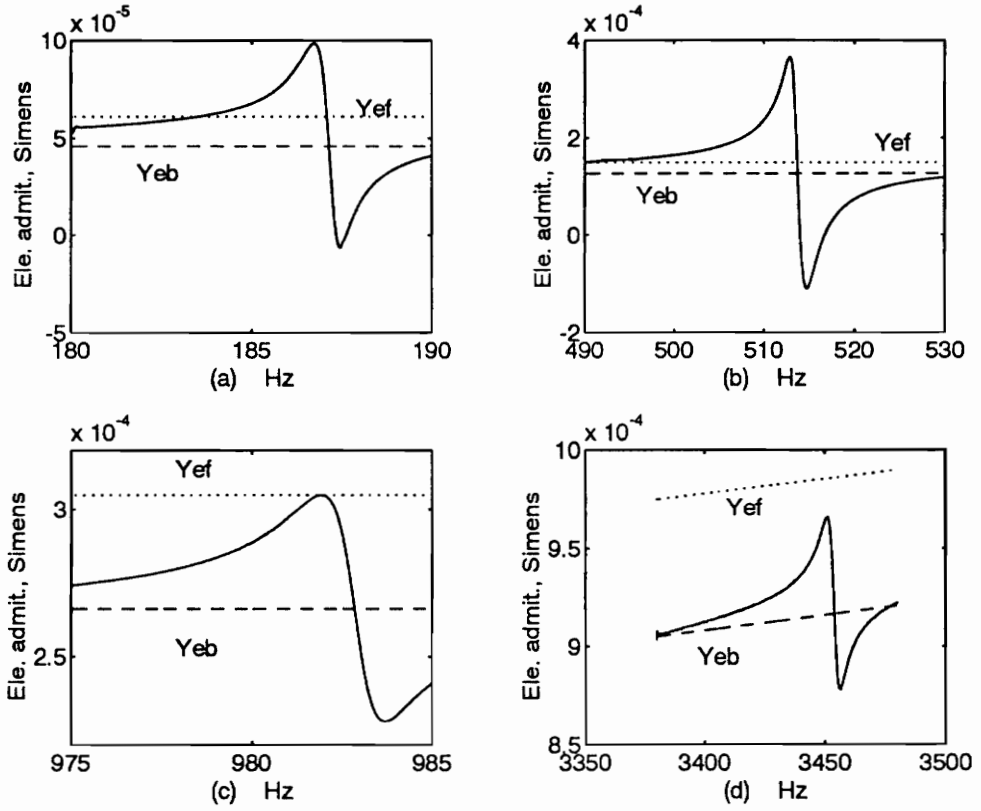

Figure 3.6 Four typical cases of the stiffening effect.

Summary

A modal analysis of a structure can be conducted conveniently, accurately and economically with surface-bonded piezoceramic patches as active sensors. The measurement of electric admittance of the PZT sensor-actuator has been proven to be an efficient and simpler method to acquire the mechanical frequency response function of a structure. Applying the proposed extraction algorithms to the measurement data can remove the stiffening of the actuator on the structure, yielding refined estimations of modal damping and structural natural frequencies. The beam example reveals the needs for natural frequency correction under some circumstances and demonstrates the effectiveness of the electromechanical approaches in removal of the impact of the PZT on the measured natural frequencies of the structures.

Chapter 4

Structural Health Monitoring Using Active PZT Sensors

This chapter presents an application of embedded PZT active sensors for structural health monitoring. The technique is based on structural signature variation with damage. However, unlike other signature-based techniques, it uses piezoceramic (PZT) patches bonded to a structure as integrated active sensors to acquire the acoustic signature of the structure. Structural damage is estimated by comparing the current electric impedance with the original data by appropriate algorithms. Two issues, the sensing localization and the sensor temperature sensitivity, which are critically associated with this technique are addressed. A novel approach of sensor temperature compensation by probability correlation function is presented. An assembled 3-bay truss structure is employed as a test bed for the study of sensing localization, sensor temperature compensation and implementation of an automated health monitoring system.

4.1 Vibration Signature-Based Health Monitoring Techniques

Nondestructive evaluation of structural integrity, or permanent health monitoring, of important structures, such as space structures, aircrafts and steel bridges, is of great interest in the aerospace, aviation and civil engineering communities. To date, extensive effort has been made to detect damage in a structure by means of vibration signature

identification. The previous work can be divide into two categories. One is the experimental modal testing approach. The theoretical basis is that the structural damage generally results in a decrease in the dynamic stiffness and an increase in damping of a structure. Since the stress distribution along a structure is different for each vibration mode, any macroscopic damage would affect each mode differently, depending on the location of the damage (Tavares and Kosmatka, 1993; Peterson and Alvin, 1993; Lindner and Twitty, 1992). This approach usually involves substantial computation. Yet, it is effective only when the damage is comparable to the size of the structure. Among the many different approaches developed, few of them exhibit engineering feasibility because of the low reliability in locating the damage and the requirement of complicated modeling, intensive computation and sophisticated transducers and instrumentation. The other category is the acoustic signature approach. Incipient damages, such as tiny cracks and loosened joints in structures can be detected more effectively by a measurement of stress wave propagation and reflection. A higher frequency range should be used in order to enhance the ability to detect damage at a microscopic level, as the wavelengths need to be short enough to be contained within the size of the damage. However, this technique needs special transducers that are able to acquire the acoustic signature of the structure in the hundred kilo-Hertz range, which is beyond the operation range of most conventional transducers such as accelerometers and force gauges, or impedance heads, etc. Furthermore, in order to implement a real-time monitoring system on a large structure

with hundreds of spots that need to be sensed, the sensor system must be non-intrusive to the structure being monitored.

As shown in the previous chapters, the piezoceramic active sensor along with electric impedance measurement, once again provides a solution for this challenge. The surface-bonded PZT active sensor is able to non-intrusively interrogate structures at an ultrasonic frequency band that is essential to the detection of incipient damage. They also feature low electric power consumption and negligible weight and stiffness compared to the structures. This makes a multi-location and real-time health monitoring of large structures practically feasible.

4.2 Structural Signature Acquisition by Electric Impedance Measurement

The model of the electromechanical interaction of the actuator with the structure, once again, is to be modified to accommodate the needs of this new application, as shown in Figure 4.1. The governing equation in terms of the structural impedance, Z_s, is presented

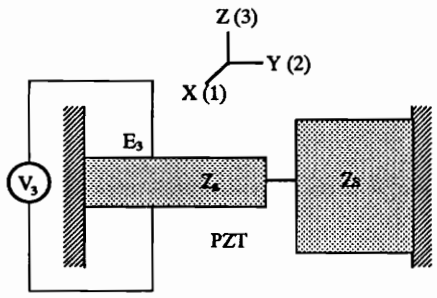

Figure 4.1 Impedance model of electromechanical coupling

here again for the convenience of discussion:

$$Y_e = i\omega a[\varepsilon_{33}^T(1-i\delta) - \frac{Z_s(\omega)}{Z_s(\omega)+Z_a(\omega)}(d_{31})^2 Y], \tag{4.1}$$

where all the definitions remain the same as in previous chapters. Here, the first term in Equation (4.1) is the capacitance admittance of a free PZT, and the second term is the result of the electromechanical interaction of the PZT with the structure. For a PZT actuator bonded to a structure, Z_a is a known linear function of the frequency. Therefore, this coupled electric admittance is uniquely determined by the structural impedance Z_s at the point of attachment. In other words, the admittance Y_e fully maps the structural signature through electromechanical interaction. Equation (4.1) can also be rewritten as:

$$Y_e = \omega a(\delta\varepsilon_{33} - y_r) + i\omega a(\varepsilon_{33} + y_i), \tag{4.2a}$$

where

$$y_r = \frac{Z_s^r(Z_s^r + Z_a^r) + Z_s^i(Z_s^i + Z_a^i)}{(Z_s^r + Z_a^r)^2 + (Z_s^r + Z_a^r)^2}(d_{31})^2 Y \tag{4.2b}$$

and

$$y_i = \frac{Z_s^i(Z_s^r + Z_a^r) - Z_s^r(Z_s^i + Z_a^i)}{(Z_s^r + Z_a^r)^2 + (Z_s^r + Z_a^r)^2}(d_{31})^2 Y. \tag{4.2c}$$

y_i and y_r are the coupling terms of the electric admittance; Z_s^r, Z_a^r, Z_s^i and Z_a^i are the real and imaginary parts of the structure and actuator impedance, respectively. As one can see, either y_i or y_r uniquely represents the signature of the structure and may be used to identify the structural damage. In practice, it is found not necessary to strip the capacitaive components of the electric admittance. Instead, they may be directly used for

damage assessment. It is also found that the real part of the admittance is more sensitive to the structural damage and more reliable for damage assessment. The mechanism of this phenomenon is that the structural damage, as a friction-damping source, will result in more real power consumption for vibration. The real power consumption is related to the real part of the admittance, but is independent of the imaginary part. Furthermore, the real part of the admittance allows for a larger dynamic range than the imaginary part for presenting the interaction components. From Equation (4.2a) one can see both the real and imaginary admittance of the PZT is a linear function of frequency ω, the real part has a much smaller slope than the imaginary part as $a\varepsilon_{33}$ is much larger than $a\delta\varepsilon_{33}$ (δ is typically less than 1%). In other words, for the imaginary part, the mechanical modulation to the electric admittance will be "drowned" in the baseline of the capacitance. This may reduce the resolution in signature pattern identification. Therefore, for signature identification purposes, the real part of the admittance is preferable.

4.3 Health Monitoring of a Space Truss Structure

4.3.1 Truss Structure And Instrumentation

Damage detection by signature pattern identification is based on the fact that the mechanical point impedance of a structure, or the electric admittance of the active sensor, which is functionally equivalent in this case, is a function of the structural integrity. Each

part of the structure contributes to the impedance to some extent. Any variation in the structural integrity will generally lead to changes in the measured electric impedance of the sensor. In a solid structure or a structure with high spatial mass density, however, there is little feasibility for implementing this approach as the stress wave may propagate eventually in infinite numbers of paths. On the other hand, an assembled truss provides an ideal test bed for this approach because of its unique structural configuration.

Figure 4.2 is a typical 3-bay aluminum Brussels space truss. The truss consists of tube struts, and spherical balls, called Delrin balls. Each strut member has a threaded connector on both ends. The members are assembled by Delrin balls through its threaded tape holes to form an interconnected frame. For a node, the connection of each strut

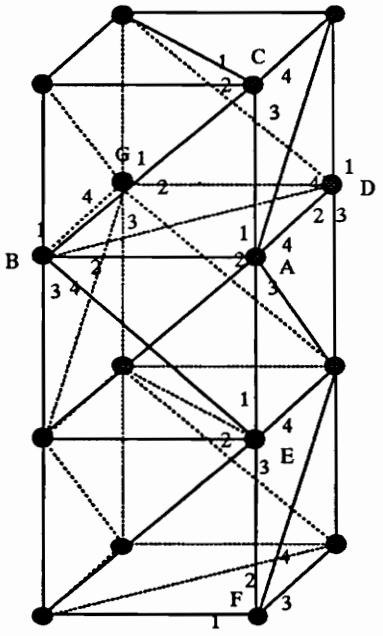

Figure 4.2 Assembled 3-bay truss

member to it can be considered as a boundary support independent of the others. The variation of the boundary condition in any member connected to this node can be detected through the change in the mechanical signature of the ball. The damage of the truss in testing is simulated by loosening the connector thread so that the test can be repeated over and over. The structural details and instrumentation are illustrated in Figure 4.3.

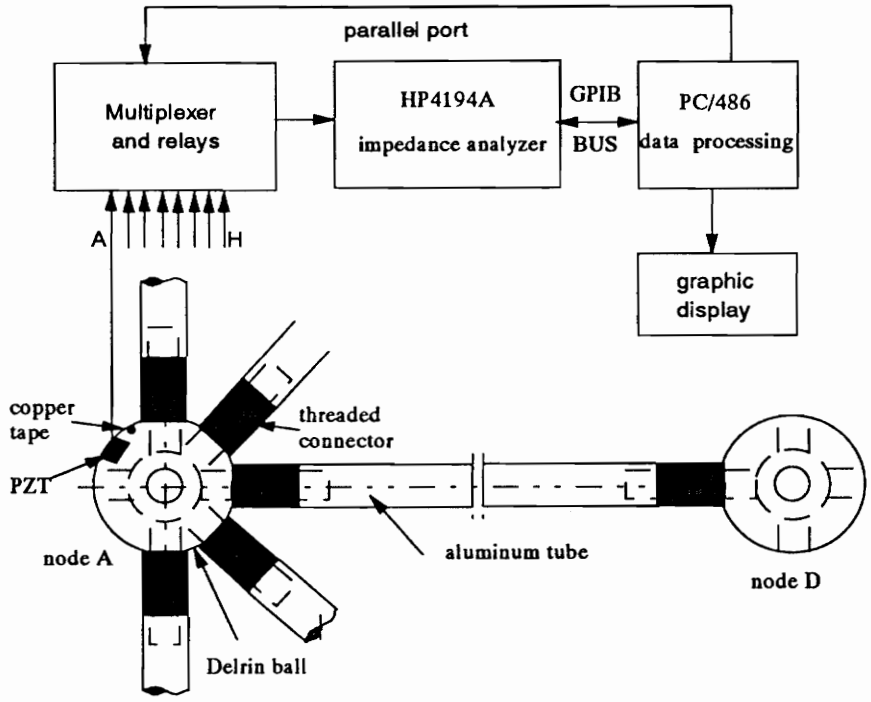

Figure 4.3 Test set-up and instrumentation for truss structure.

Eight PZT sensors of 7×7×0.19 mm are bonded to ball A through ball H, respectively. All the sensors are hooked up to a relay switch box multiplexed by a PC through its parallel port. Each sensor is switched on to the HP4194A electric impedance analyzer in turn for measurement of its electric impedance. The data is then transferred to the PC through a

GPIB bus for numerical processing, and the result regarding the integrity of each node is graphically displayed on the screen. All of the control, communication and display are coordinated by a dedicated program written in QBASIC. The impedance patterns of each sensor under healthy conditions and severe damage conditions are taken and saved in advance. Their difference in frequency domain is calculated and saved as a reference for evaluating damage. An appropriate threshold is predetermined based on the large quantity of test data statistically processed.

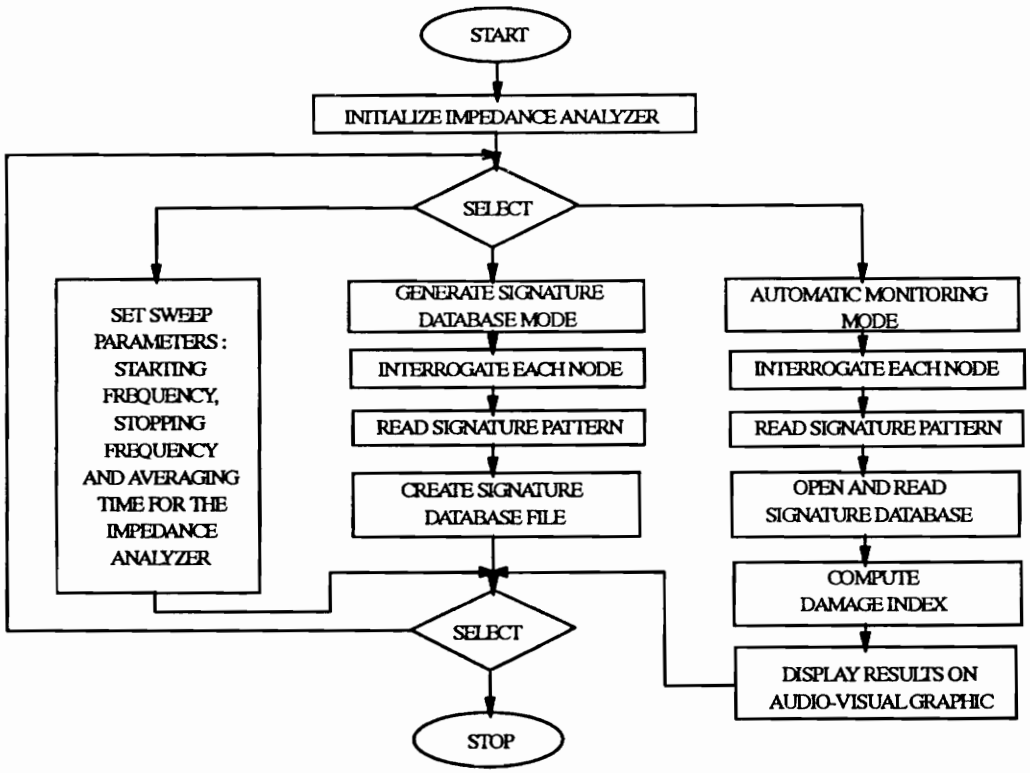

Figure 4.4 Flow chart of the automated health monitoring control algorithm.

During the scanning of each node, if the relative deviation in the electric admittance pattern of a node is found to exceed the threshold, the corresponding graphic node(s) on the monitor screen will change color and an audio alarm signal will be given at the same time. Entire scanning of all eight nodes takes about 1.5 minutes. The system flow chart is given in Fig. 4.4. The monitoring parameters, such as frequency range, sweep rate and excitation signal level, can be remotely set up from the computer. The frequency band from 80 kHz to 120 kHz for this truss is selected as it is found to be fairly sensitive to the integrity of the nodes.

4.3.2 Damage Index

The signature deviations may be quantitatively described by a damage index, defined as the area difference between the signature patterns of a healthy structure and a damaged structure normalized to a preset (reference) value. This value is determined by the maximum signature pattern variation that could possibly occur. For the truss, this is the difference between a completely loosened connector and a securely tightened connector. As the signature pattern of a ball at an ultrasonic band exhibits a nearly random nature, the mean-square algorithm is used to calculate the relative deviation (*RD*):

$$RD_i = \frac{\sum_{j=1}^{N} (\mathrm{Re}(Y_{ij}^1) - \mathrm{Re}(Y_{ij}^0))^2}{\sum_{j=1}^{N} (\mathrm{Re}(Y_{1j}^1) - \mathrm{Re}(Y_{1j}^0))^2}, \qquad (4.3)$$

where Y_{ij}^1 and Y_{ij}^0 are the admittance of each PZT sensor at frequency interval j. The first subscript i indicates the *ith* connector; the superscript 1 designates the status of a ball under interrogation, with *0* signifying a healthy condition. Y_{1j}^1 and Y_{1j}^0 are the admittance when connector 1 is seriously damaged (completely loosened) and when it is in good condition (tightened), respectively. N is the number of frequency intervals which is 401 for the HP4194A analyzer. As the PZT sensor is deliberately placed closer to the first connector of each node, it is generally true that the RD_i is equal to or less than the unit. This notation will be found convenient for the description in damage assessment. During the monitoring, if the damage index of a node is found to be excessive, it is safe to say that there is something wrong with this node, or with its surrounding strut members.

4.3.3 Localization of Damage Sensing

A question occurs at this point as to how reliable this damage index is in representing the true damage level of the node being interrogated. Will it be contaminated by the damage or structural variation of other nodes? Will the normal operating condition change, such as the static loading or boundary condition of the whole structure, result in any significant variation in the index? To have a full understanding of this issue, the detection range of

the sensor has been experimentally investigated. The node A is selected as a check point as it is in the middle of the truss. The electric admittance of the PZT at node A are taken when connector 1 at node A is tightened and then completely loosened. Their difference is calculated as the denominator of the damage index (*RD*). The electric admittance of the PZT actuator is then measured repeatedly when each connector at node A to H is loosened by 1/4 turn. The electric admittance are given in Appendix B, from which it can be seen that the influence of each connector on the electric admittance decreases rapidly with increasing distance from the node A. The graphic summary of a quantitative analysis based on the previous definition of *RD* is given in Figure 4.5. The signature variation resulting from loosening connector 1 at node A is taken a reference. By definition, *RD* for connector 1 at node A is a unit while other RDs are less than one as the impact of a loosened joint is expected to decay with distance.

Figure 4.5a shows the average *RD* for all connectors at each node. The horizontal coordinates 1-7 correspond to nodes A-G. It can be seen that the impedance of node A to which the PZT sensor is bonded is heavily impacted by the conditions of its adjacent members. Comparatively, the impedance is much less influenced by the conditions of the members at nodes B, C, D and E (average *RD* one order lower). For nodes F and G, this influence becomes even more trivial as they are both two struts away from node A. Figure 4.5b shows the deviation of the *RD* with 4 adjacent members at each node. All the members directly attached to node A exhibit much greater influence than the members

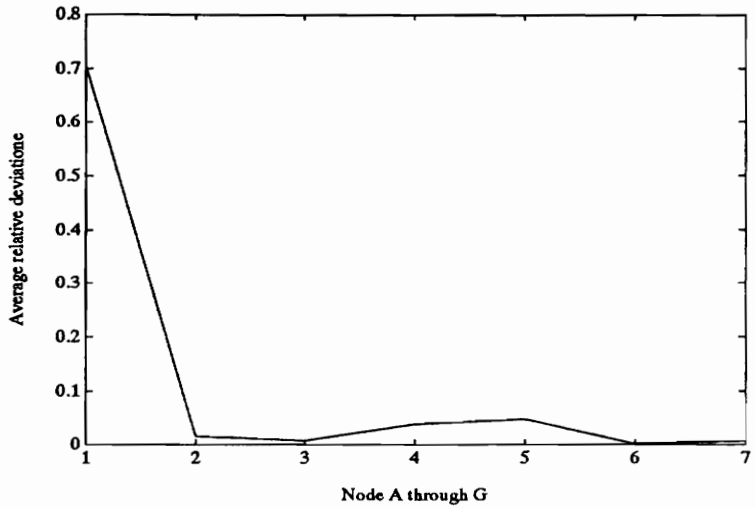

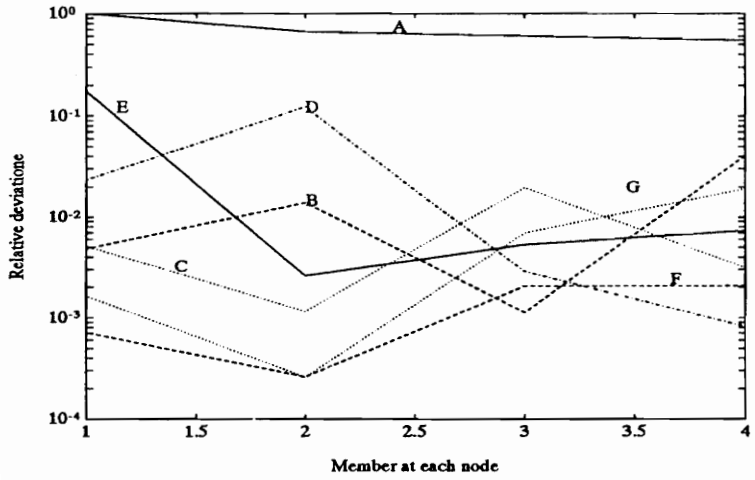

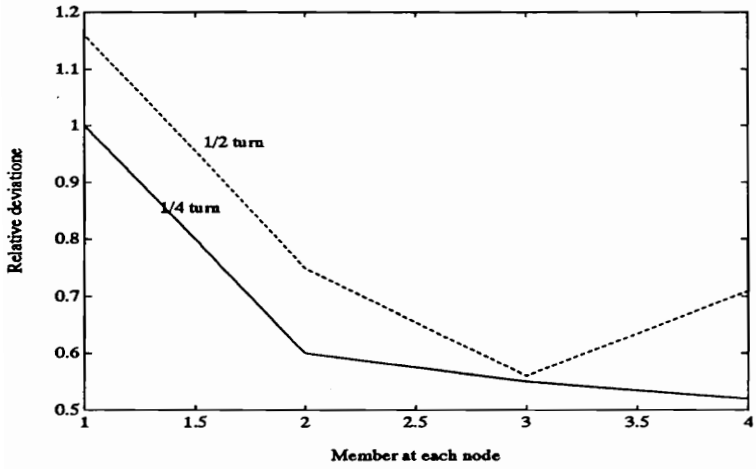

Figure 4.5 Plots of relative deviation (RD)

attached to other nodes with no exception. This shows a clear picture of the sensing range of the PZT sensor. It is primarily limited to the immediate vicinity of node A. The integrity at other nodes make little contribution to the signature pattern of node A. This "locality" of the detection enables us to monitor a truss on a one-to-one basis, that is, each sensor is able to only monitor the structural integrity of the node it is residing on and the result will not be contaminated by the damage occurring elsewhere.

Similar vibration localization phenomena on periodic structures, that is, the structures made of identical substructures or bays, have previously been investigated and reported (Bendiksen, 1989; Bouzit and Pierre, 1993). For an assembled truss, the localization effect of sensing may be interpreted by the friction damping at each joint connection, the net configuration of the truss structure and the local vibration modes at ultrasonic frequencies (Sun et al., 1994). First, all the joint surfaces of each member constitute friction dampers in series. The stress wave generated at node A by the active PZT sensor is completely constrained in the line of a member during its propagation, and is forced to pass each damper along the way out. This damps out the stress wave much more quickly than it would in a solid continuum and allows little energy to be transmitted to neighboring nodes. As the detection of the structural damage depends on the reflection of the stress wave back to node A, the stress energy level at the location of damage is critical to the sensitivity. Second, the radiation configuration of the truss structure dissipates the stress energy exponentially and three dimensionally. As one of the supporting borders to

node A, each immediate strut member provides its share ($1/m$, where m is the number of members connected to the node) of boundary impedance to the node ball. This share of mechanical impedance in turn consists of the impedance of this member and the impedance provided by all the members at the neighboring node (for instance, node D). Therefore, the impedance contribution of each member at node D to node A is approximately $(1/m)^2$. For a node n members away from node A, the contribution would be approximately $(1/m)^{n+1}$. Finally, this sensing locality can also be interpreted as the result of ultrasonic excitation. Under such high frequency, no vibration will appear except the local modes, which will cause little deflection of the node ball beyond its immediate vicinity.

The sensing localization phenomenon greatly facilitates the determination of damage location in a complex structure as well as the determination of an appropriate threshold for damage assessment. It also allows for a quantitative assessment of the damage severity to some extent. For a particular structure, once the maximum possible "noise table" from other node is determined (in this truss, it is less than 5%), it is natural to set the threshold for alarming above that value. The damage extent may be roughly estimated by the variation in the damage index between unit and the noise table. The extent of the damage in this truss case is simulated by controlling the number of turns when loosening a connector. 1/4 turn is made to all the connectors during the above localization test. Then an additional 1/4 turn is made to the 4 connectors around node A. As a result, the *RD*

values for these members increase, as shown by Figure 4.5c. However, as one can see, this positive correlation does not occur consistently with all the members. For connector 3, the *RD* almost remains the same, not to mention the proportionality. This result implies that trying to assess the damage extent quantitatively by simply reading the *RD* value is generally not promising. It seems more realistic to establish threshold values through statistical analysis and make an estimation of the damage extent based only on the status of "acceptable or unacceptable."

4.3.4 Temperature Compensation by Cross Correlation Function

The material properties of piezoceramic exhibit fairly strong temperature dependency. The temperature coefficient of dielectric constant for G1195 PZT is about 0.3%/C°. When bonded to a structure, its electric impedance, both the interaction part and the capacitive part are subject to change with temperature according to Equation (4.1). In addition, the structural property variation with temperature also manifests itself as shift of mode peaks in the electric impedance. Experiments show that even a temperature variation under a laboratory environment could result in an *RD* change of the same order as those resulting from moderate structural damage. This thermal drift may easily lead to an erroneous conclusion regarding the structural integrity if not properly corrected.

Instead of pursuing compensation by a secondary compensation sensor, a numerical method is sought to solve the problem. Study of the signature patterns shows that there is a significant distinction in the electric impedance variation caused by the thermal drift and that caused by structural damage. Temperature change causes almost uniform vertical drift of the capacitance line and horizontal shift of most structural modes in the electric admittance. That is, the entire signature pattern essentially translates vertically and horizontally. On other hand, the impedance variation due to structural damage is somewhat "local and abrupt" disturbance on the signature pattern without much change in baseline. This feature allows for separation and removal of the temperature effect from the electric impedance by numerical manipulation.

Correction for this type of variation is something that is much easier for human intelligence than for a machine. The acoustic signature pattern of a structure within the ultrasonic band exhibits nearly a random nature. To determine the extent of the horizontal (thermal) shift of the impedance pattern, the random function correlation approach is employed. The cross-correlation function between two random series is defined as (Bendat and Piersol, 1980):

$$R_{XY}(n) = \frac{1}{N}\sum_{1}^{N} X(r)Y(r+n), \tag{4.4}$$

where X and Y are two sets of discrete random time series, and n is the number of data points delayed. The cross-correlation coefficient is:

$$\rho_{XY}(\tau) = \frac{R_{XY}(\tau)}{\sqrt{R_X(0)R_Y(0)}} \tag{4.5}$$

where $R_X(0)$ and $R_Y(0)$ are the auto-correlation functions of X and Y, respectively. If X is identical to Y, except being delayed by time τ_t, then their cross-correlation coefficient $\rho_{XY}(\tau_t)$ must equal to unit. By the same token, if the damage impedance Y_e equals the healthy impedance X plus a temperature drift of n data points and an uncorrelated damage influence, then $\rho_{XY}(n\Delta\tau)$ will reach its maximum at a delay $n\Delta\tau$. When the electric impedance under interrogation is being translated through minus n data points with respect to the healthy one, two patterns should completely coincide except for the portion resulting from true damage.

The vertical translation is simply corrected by the difference in the mean value of the original and the interrogated patterns. This simple numeric processing greatly reduces the temperature effect. Figure 4.6 illustrates the real electric admittance of node A. (a) is the original signature and the signature after thermal drift. In this case, the temperature drift results in about a 56% change in the RD value due to an ambient temperature variation of 35°F. Figure 4.6 (b) is the signature after vertical translation. The *RD* decreases by only 3%. By applying cross-correlation analysis to them, a horizontal shift of 4 data points is detected, as indicated by the peak coordinate of Figure 4.6 (c). The drifted signature is then moved forward 4 data points. This brings the *RD* down to 15% - a level of the noise

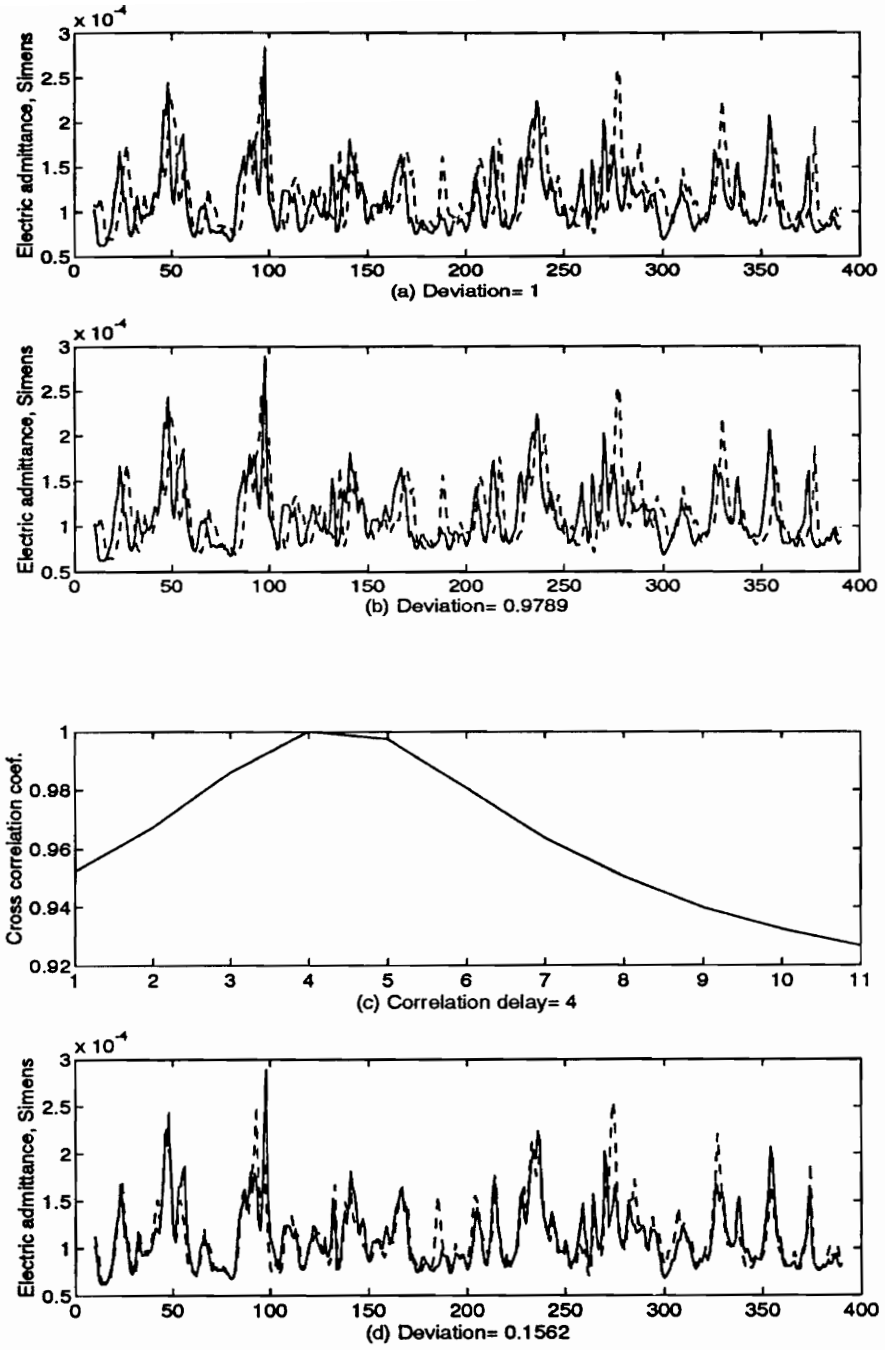

Figure 4.6 Numeric compensation of electric admittance thermal drift

(a) original;(b) after vertical translation; (c) cross correlation coefficient; (d) after complete compensation (solid line-original, dashed-line drifted).

table of cross talk between nodes whose impact can be easily manipulated by selecting an appropriate threshold for alarming.

Strictly speaking, this cross-correlation-based compensation is valid only when the impedance variation is solely due to the temperature change. The effective use of this numerical manipulation relies on the fact that the temperature contribution to the impedance change is significantly greater than the structural damage. If the damage change, which does not follow the simple translation rule at all, is overwhelming, the estimated delay n will no longer reflect the true thermal shift, and the correction is expected to be less effective, or even collapse. However, this case did not occur in the truss experiment.

4.3.5 Selection of Monitoring Parameters

4.3.4.1 Frequency Range

The sensitivity of detection, or the variation in the impedance pattern due to the structural integrity change, is closely related to the frequency band. It should be selected to include most of the vibration modes of the Delrin ball under its full boundary support, typically in the range of a few hundred kHz. Therefore, any structural change in the member will manifest itself in the measured admittance of the node as a shifting-up or shifting-down of

certain major modes, or a creation or disappearing of certain modes. The frequency range is basically determined by trial-and-error as there is little analytical work that can be done regarding the vibration modes of such complex structures at ultrasonic frequencies. Experiments show that a frequency band with high modal density is always favorable as it generally covers more boundary condition information. In addition to that, higher frequency is found to be preferable in localizing the sensing. This is due to the fact that structural damping is more effective at high frequency.

4.3.4.2 Excitation Level

The voltage level under which the electric admittance is measured and its effects on the detection sensitivity and localization has also been also investigated. Excitation levels higher than 2.8 V_{p-p} is not available on the HP4194A analyzer, as it is designed for weak-field measurement. Therefore, an auxiliary test was conducted on a standard signal analyzer (Zonic WCA) to experimentally check the impact of the excitation level on the localization effect and sensitivity. The voltage and current of the PZT are externally measured and the electric admittance was calculated under different excitation levels. Up to 28 V_{p-p} excitation is applied, which is supposed to be the top limit of the PZT's linear range. There is no noticeable difference observed compared with the result of 2.8 volt excitation. This agrees with the theory of linear systems. Therefore, it is safe to say that under certain excitation levels, "the sensing radius" is uniquely determined by the

structure's configuration and the location of the PZT. Varying excitation voltage will generally not change the impedance pattern except improving the signal-to-noise ratio, which may improve the capability of identifying weak modes. However, the PZT material properties are known the functions of electric field intensity. A further increase in excitation level will certainly result in a noticeable difference in the baseline of the admittance. This should be avoided in the selection of the voltage level when high voltage levels are available with the analyzer.

Summary

Multi-location and real-time health monitoring of large space structures can be feasibly implemented by the use of surface-bonded PZT active sensors and electric impedance measurement. The high sensitivity of the surface-bonded active PZT sensor is the key to the detection of incipient damage. Localization of the sensing plays an important role in the damage location determination of a real-world structure. The tiny size and negligible weight of the sensors allow for non-intrusive and permanent monitoring of the structure. The system uses a simple statistic algorithm for signature pattern identification, minimizing computation facilities. The thermal drift of the electric impedance of the embedded PZT sensors can be effectively corrected for by a cross-correlation function approach. However, the assessment of damage severity at a higher resolution still need to be investigated.

Chapter 5

Determination Of Electromechanical Energy Conversion Coefficients of PZT Actuators

The energy conversion efficiency of a piezoelectric actuator is of great interest for those involved in active vibration control of aerospace structures by means of embedded actuators, as the power consumption and weight of the power supply are a major concern. The electromechanical coupling coefficient of PZT, although related, does not represent the overall efficiency of a transducer as it does not take into account the electrical and mechanical losses. An experimental scheme for the determination of the conversion efficiency of a PZT stack actuator is presented. It directly measures the input and output energy under impulsive actuation and calculates the efficiency by its definition. A commercially-available stack actuator is investigated. The data thus obtained represent the overall efficiency of a PZT stack actuator for impulsive actuation or steady-state actuation at its resonance frequency. It is significantly lower than its nominal material coupling coefficient, but higher than that calculated by the resonance-antiresonance method.

5.1 Motivation

The energy consumption and the energy conversion efficiency of a piezoelectric actuator used in an active control system are one of the most fundamental concerns regarding the

viability of active control for applications that are weight and volume sensitive, such as noise control of aircraft and vibration reduction of space structures. A substantial research effort has been made in the last few years to understand the energy allocation within capacitive piezoelectric actuators during actuation. Recent efforts involve analytical investigation of the energy efficiency of embedded PZT actuators (Liang, Sun and Rogers, 1994; Stein, Liang, and Rogers, 1993). The power consumption of an integrated PZT stack actuator has been also studied (Flint, Liang and Rogers, 1994). The previous research shows that the actual efficiency of a PZT actuator is always lower than what the nominal conversion efficiency, or the coupling coefficient of the material, implies under dynamic operation. However, little has been done to experimentally determine the actual efficiency of a PZT actuator by either researchers or manufacturers.

The energy conversion efficiency of a reactive transducer involves both reactive power and dissipative power. To improve the total efficiency, we need to improve the power factor and reduce the power dissipation of the transducer. Piezoelectric actuators are typically driven by a high-voltage amplifier to maximize the displacement output. For ac operation, being able to know the true energy conversion efficiency of an actuator is of great interest to engineers who need to choose an appropriate power supply. An ac amplifier that has high output voltage usually provides very limited current. The power consumption of a PZT actuator is proportional to the operating frequency. Saturation of an amplifier occurs when the actuator is trying to draw too much current. This saturation

frequency depends on the apparent power rating of the amplifier once the efficiency and power factor of the actuator are known. If the required mechanical power from the actuator is known, the minimal power rating of the amplifier can be estimated by the actuator efficiency.

The electromechanical coupling coefficient of piezoelectric material, when operated in direct mode, is defined as:

$$k = \sqrt{\frac{\text{mechanical energy converted}}{\text{electric energy applied}}}. \qquad (5.1)$$

A k value of 0.7, which is typical for many PZT materials, means that for each Joule of electrical energy applied to a PZT, one-half Joule is converted into the mechanical strain energy of the PZT as it expands or contracts under an electric field. The other half Joule will remain in the PZT as electrical field energy. Apparently, the coupling coefficient is related to the power factor, but not to the dissipation. The coupling coefficient is typically determined by measuring the resonance and antiresonance frequencies of a PZT specimen with a standard geometry. The coefficients thus obtained do not represent the overall efficiency of the electromechanical transduction of the PZT actuator, since they do not take into account the electrical and mechanical dissipation of the PZT. Furthermore, the coupling coefficient is a constant, but the actual conversion coefficient of a reactive actuator is a function of frequency. The interesting thing is that while the power factor and the dissipation play a opposite roles in the overall efficiency, both peak at the

resonance frequency and minimize at the off-resonance frequency of the actuator. Thus, the improvement in the efficiency by the power factor increase may be canceled out partially by the increase in dissipation at resonance frequencies. A low power factor at off-resonance may still lead to a good overall efficiency because of low dissipation. In addition, commercial PZT actuators typically have steel casing. This introduces additional mechanical dissipation and structural dynamics and further lowers the conversion efficiency. As a result, the overall efficiency is a complicated function of the coupling coefficient, operating frequency, material dissipation and structural dynamics. For an end user, an overall conversion efficiency that is experimentally determined in a situation close to the real application and that has taken into account all the influencing factors is more meaningful than an analytical estimation.

Direct measurement of energy transduction and determination of the efficiency by its definition eliminate all unknown factors and result in data that is more representative of the performance of an actuator in a real application. The approach presented is based on the general principle of energy conservation during electromechanical transduction. The conversion coefficient of an actuator is determined by direct measurement of the mechanical energy and the electrical energy and indirect estimation of the energy loss by the material coupling coefficient and equivalent circuit model.

5.2 Determination of Energy Conversion Coefficient of a PZT Stack Actuator

5.2. 1. Principle of Measurement

The method presented uses the impulsive electrical energy discharge as a vehicle because it is easy to obtain a precise measurement of electrical field energy. Figure 5.1 schematically illustrates the principle of the measurement scheme. A PZT actuator is essentially a capacitor (designated by C_2) with the capability of converting electrical energy to mechanical energy. A working capacitor, C_1, charged up by a dc power source

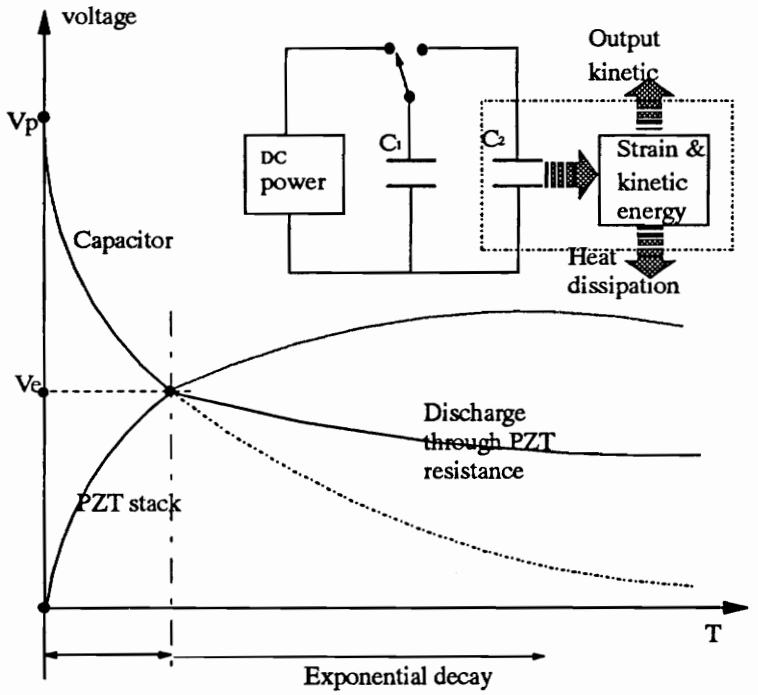

Figure 5.1 Determination of electrical energy converted to mechanical energy

to a voltage, V_p, discharges through the actuator when the switch is toggled. The charge

and discharge ends when an equilibrium voltage, V_e, is reached, and the residual electrical energy continues to discharge, but now through the leakage resistance of the capacitance. The electrical energy transferring during this process may be determined easily if V_p and V_e are measured. Meanwhile, as a result of the piezoelectric effect, the actuator impulsively expands to its maximum deformation and then contracts to its original dimension as the discharging through the leakage progresses. The impulsive movement of the actuator also builds up kinetic energy in the actuator and the structure being actuated. If all the mechanical energy gain and the electric voltages are measured, then the overall efficiency of the actuator can be determined.

5.2.2 Analysis of Energy Allocation

The energy decrease of the working capacitor, C_1 ,during discharging is:

$$\Delta E_{c1}^{e} = \tfrac{1}{2} C_1 (V_p^2 - V_e^2) . \tag{5.2}$$

The total energy converted from electrical form to mechanical form by the actuator can be expressed as:

$$E_t^m = \Delta E_{c1}^{e} - E_{c2}^{e} - E_{r1}^{e} - E_{r2}^{e}, \tag{5.3}$$

where $E_{c2}^{e} = \tfrac{1}{2} C_2 V_e^2$ is the electrical field energy stored in the capacitance of the actuator, and E_{r1}^{e} and E_{r2}^{e} are the energies dissipated in the equivalent resistance of the capacitor and the actuator, respectively. The superscript e indicates electrical and m mechanical. The

total mechanical energy converted splits into three parts: the strain energy of the actuator, the kinetic energy of the actuator (including the kinetic energy of the object driven by the actuator), and the mechanical dissipation of the actuator:

$$E_t^m = E_{strain} + E_{kinetic} + E_{loss}. \tag{5.4}$$

The total electrical input to the actuator is the energy loss of C_1 minus the dissipation on its internal resistance:

$$E_{in}^e = \Delta E_{c1}^e - E_{r1}^e. \tag{5.5}$$

The total efficiency of electrical-to-mechanical energy conversion of the actuator is defined as:

$$K_t = E_t^m / E_{in}^e \quad . \tag{5.6}$$

Similarly, the coefficients of converting electrical energy to kinetic energy and strain energy can be expressed as:

$$K_k = E_{kinetic} / E_{in}^e \tag{5.7}$$

and

$$K_s = E_{strain} / E_{in}^e. \tag{5.8}$$

The percentages of the dissipated energies in the mechanical damping and the electrical resistance of the actuator are (E_{r2}^e will be defined later):

$$K_l = E_{loss} / E_{in}^e \tag{5.9a}$$

$$K_e = E_{r2}^e / E_{in}^e. \tag{5.9b}$$

5.2.3 Test Apparatus

Figure 5.2 is a schematic diagram of the experimental set-up for the determination of the conversion coefficients of a P-245.70 PZT stack actuator made by Physik Instruments. The actuator is made of a PZT stack rod 10 mm in diameter, housed in a stainless steel casing. The stack rod is prestressed by 5 washes to keep it from being stretched. The actuator is vertically mounted on a bulky steel platform. A steel ball is placed on the top of the actuator output shaft to determine the kinetic energy output as well as the velocity of the shaft. A high voltage dc power supply is used to charge a metal film capacitor of 0.50 MF. The capacitor is switched between the dc power supply (Atomic 1316) and the stack for repeated charge and discharge. During the discharge of C_1, the shaft of the actuator expands momentarily and drives the ball upward into the air. The trajectory of the steel ball is monitored by an eddy current proximity probe (Electro PA 11503). The strain of the stack is sensed by the built-in half-bridge strain gage (700 Ω) and an external gage conditioner (Omega P3500). The strain, the trajectory of the ball, the voltage across the PZT stack, and the charging voltage are simultaneously recorded by a multi-channel signal analyzer (Zonic WCA). Both the mechanical energy gain and the electrical energy change are then determined from the recorded signals. The PZT stack is short-circuited by a switch to release its residual charge when the impact is over so that the electrical charge will not accumulate.

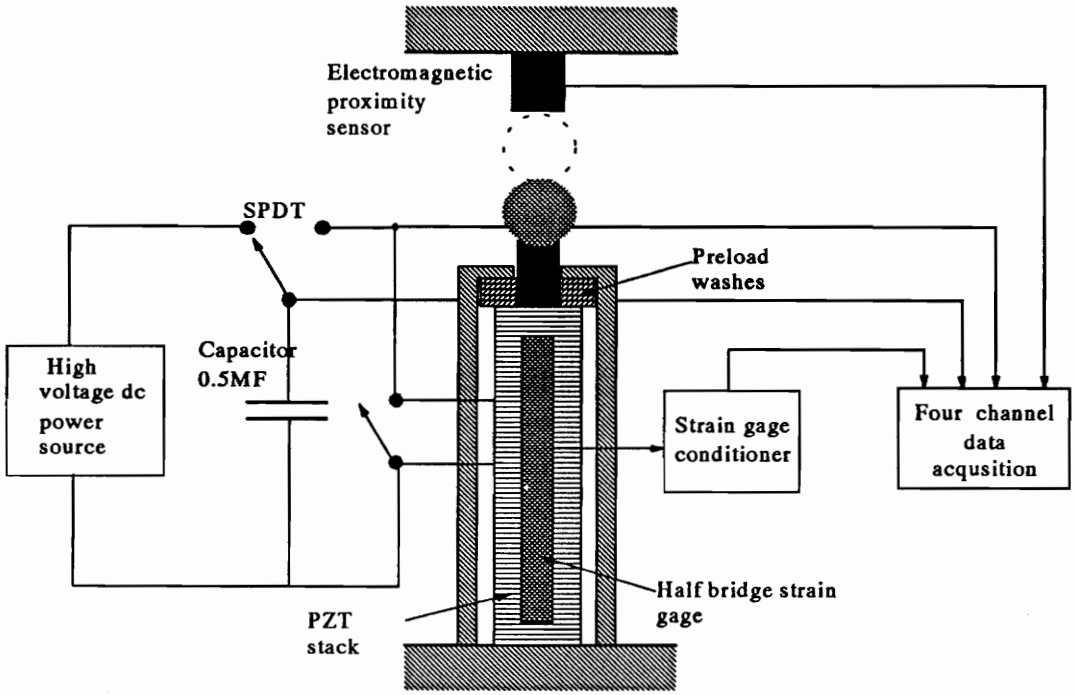

Figure 5.2 Schematic diagram of the experimental set-up

The kinetic energy of the bali gained in impact can be easily found by its peak trajectory, h:

$$E_b = mgh. \tag{5.10}$$

The strain energy stored in the stack is:

$$E_{strain} = \tfrac{1}{2} k_{stack} (\varepsilon l)^2, \tag{5.11}$$

where k_{stack} is the total stiffness of the stack rod and the preloading washes, ε is the strain of the PZT rod at the equilibrium voltage, V_e, and l is the effective length of the stack. The stack rod also contains kinetic energy as its one end moves during the actuation, and can be expressed as:

$$E_k = \frac{1}{2} m_{se} (u_0)^2, \tag{5.12}$$

where m_{se} is the effective mass of the actuator rod, which is 1/3 of the total mass of the rod as one end is fixed, and the velocity varies linearly along its length. u_0 is the peak linear velocity of the actuator, which can be determined by Equation (5.10).

5.3 Equivalent Circuit Model and Electrical Dissipation

It is very important to understand that not all the energy reduction of C_1 during discharge is pumped into the stack as indicated by Equation (5.5). In fact, a substantial portion may be lost on the internal resistance of the capacitor. Accurate determination of the net electrical energy input to the actuator involves the determination of the electrical loss on the internal resistance of the actuator. Neither direct measurement nor analytical calculation from the discharging curve is feasible in terms of the accuracy, as the discharging occurs in a small fraction of milliseconds. However, an estimation can be made by use of the coupling coefficient of the PZT material and the equivalent circuit models of the capacitor and the actuator. The capacitor may be modeled as an R-C circuit since its dc resistance is almost infinite. The actuator can be modeled as an R-L-C resonator in parallel with a capacitor, as illustrated in Figure 5.3(a). To verify the models, the electrical impedance of the capacitor and the stack are measured by the HP4194A impedance analyzer and plotted in Figure 5.4 along with the simulated impedance. Good agreement between the two sets of curves indicates that the models are good

representatives of the real components for the first resonance mode. The extracted parameters of the models are listed in Table 5.1.

Table 5.1 Equivalent circuit parameters

	R, Ω	C_1, C_2 nF	C_3, nF	L, mH
Stack	9.2	502.0	31.6	67.7
Capa.	17.4	491.1	N/A	N/A

Table 5.2 Physical constants of P245.70 PZT stack actuator (Physik Instrumente, 1990)

Max. expansion at 1000 V μm	Coupling coefficient, k_{33}	Mass density of PZT g/cm^3	Stiffness K_{stack}, N/mm
120	0.66	7.7	8,300

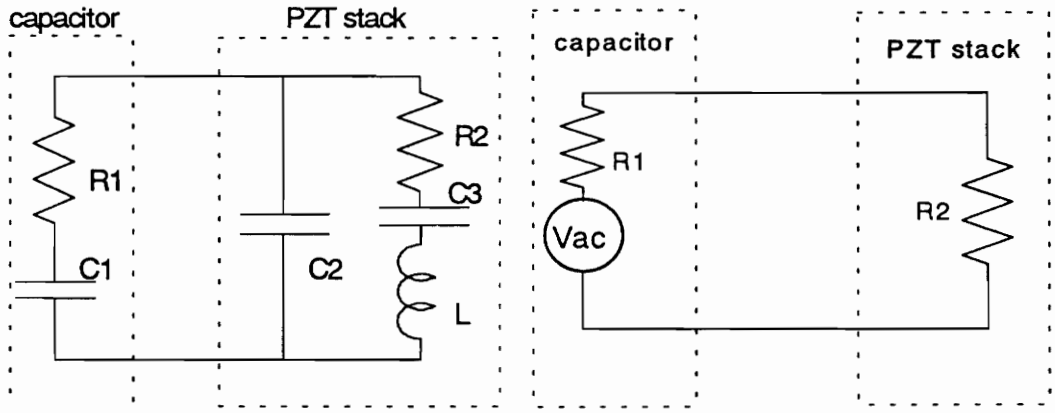

(a) General equivalent circuit (b) Reduced circuit at resonance

Figure 5.3 Equivalent circuits of stack and capacitor.

The R-L-C branch of the equivalent circuits represents the first mechanical resonance of

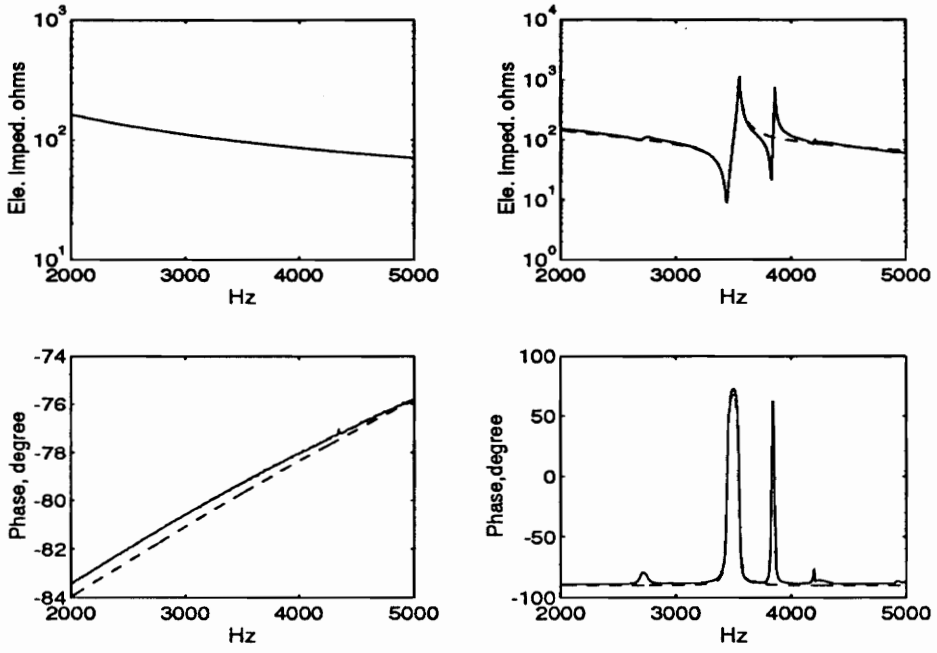

Figure 5.4 Electrical impedance of the capacitor and stack (___ measured ------ simulated)
(The left plot is the capacitor and the right plot is the actuator)

the stack. Under the impulsive charging, the branch starts a damped oscillation at it resonance frequency. As a result, its complex electrical impedance is simply reduced to resistance R_2, and the bypass effect of capacitance C_2 can also be neglected as its capacitive impedance is much larger than R_2. The resultant circuit is two resistors in series, as shown in Figure 5.3 (b). The total electrical dissipation, which is unknown yet, is then split between R_1 and R_2:

$$E_{r1}^e = E_r^e \frac{R_1}{R_1 + R_2} \text{ and } E_{r2}^e = E_r^e \frac{R_2}{R_1 + R_2}. \tag{5.13}$$

In order to determine the total electrical energy loss, E_r^e, we use the relationship between the stored electrical energy and the converted mechanical energy:

$$k_{33}^2 = \sqrt{\frac{E_t^m}{E_{c2}^e + E_t^m}} \tag{5.14a}$$

or

$$E_t^m = E_{c2}^e \frac{k_{33}^2}{1 - k_{33}^2}, \tag{5.14b}$$

and then, the total electrical loss can be expressed as:

$$\begin{aligned} E_r^e &= \Delta E_{c1}^e - (E_{c2}^e + E_t^m) \\ &= \Delta E_{c1}^e - E_{c2}^e \left(\frac{1}{1 - k_{33}^2}\right). \end{aligned} \tag{5.15}$$

By substituting Eqs. (5.13) and (5.15) into Eq. (5.5), the net electrical energy input to the stack actuator can be expressed as a function of the electrical energy change of C_1, the equivalent resistance of the capacitor, and the coupling coefficient of the PZT:

$$\begin{aligned} E_{in}^e &= E_{c2}^e + E_t^m + E_{r2}^e \\ &= \Delta E_{c1}^e \frac{R_2}{R_1 + R_2} + E_{c2}^e \frac{R_1}{(1 - k_{33}^2)(R_1 + R_2)}. \end{aligned} \tag{5.16}$$

The overall conversion coefficients can be readily calculated by Eq. (5.6) - Eq. (5.9) and Eq. (5.16).

5.4 Test Results

The efficiencies of the stack are evaluated at a variety of charging voltage levels, V_p, to investigate its effect on each coefficient. The coefficients under different mass loading (ball masses) are also measured. The results are listed in Table 5.3.

Table 5.3 Energy conversion coefficients

Ball diameter 31.75 mm (130.4 g)

V_p	K_t	K_s	K_k	K_e	K_c	K_l
600	0.350	0.104	0.128	0.200	0.450	0.118
700	0.345	0.113	0.135	0.211	0.445	0.098
800	0.341	0.120	0.139	0.222	0.439	0.082
900	0.339	0.118	0.125	0.226	0.436	0.096
Mean	**0.344**	**0.114**	**0.132**	**0.215**	**0.443**	**0.098**
Dev.%	0.49	0.71	0.64	1.17	0.62	1.30

Ball diameter 25.4 mm (66.7 g)

V_p	K_t	K_s	K_k	K_e	K_c	K_l
600	0.348	0.108	0.140	0.204	0.449	0.100
700	0.344	0.112	0.143	0.214	0.443	0.090
800	0.341	0.119	0.149	0.220	0.440	0.073
900	0.335	0.118	0.152	0.234	0.432	0.065
Mean	**0.342**	**0.114**	**0.146**	**0.218**	**0.441**	**0.082**
Dev.%	0.53	0.52	0.55	1.25	0.70	1.30

Ball diameter 19.05 mm (31.8 g)

V_p	K_t	K_s	K_k	K_e	K_c	K_l
600	0.346	0.117	0.159	0.209	0.446	0.070
700	0.342	0.120	0.161	0.219	0.440	0.061
800	0.339	0.124	0.176	0.226	0.436	0.039
900	0.332	0.124	0.169	0.231	0.439	0.039
Mean	**0.340**	**0.121**	**0.166**	**0.221**	**0.440**	**0.053**
Dev%	0.61	0.36	0.78	1.00	0.40	1.60

Figure 5.5 is the graphic presentation of the mean values of each coefficient when using the 19.05 mm steel ball.

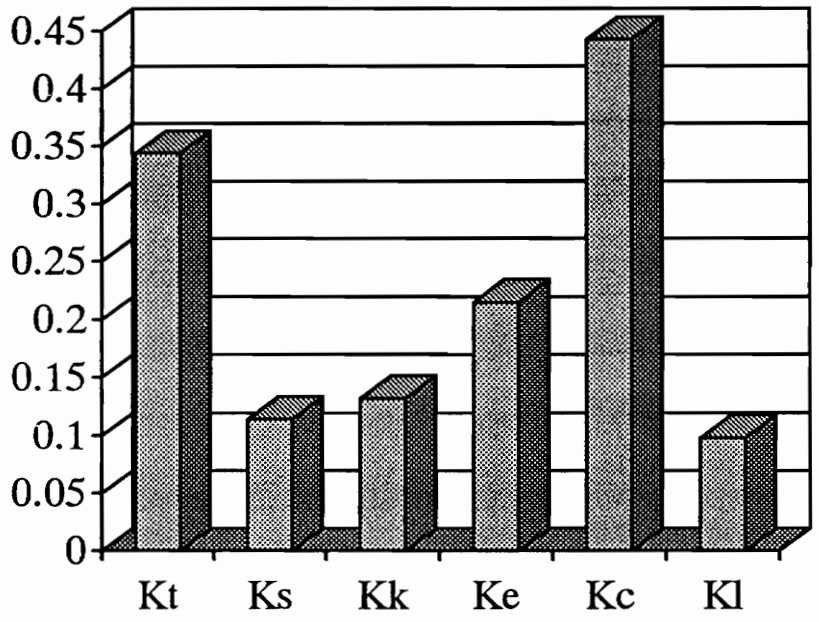

Figure 5.5 Percentage allocation of energies in PZT stack actuator

5.5 Analysis of Efficiency

The test data shows that the overall efficiency of a PZT stack actuator with steel casing under impulsive actuation is significantly lower than what its nominal coupling coefficient may imply ($K_{33}^2 = 0.43$). A substantial portion of input electrical energy (22%) is dissipated on the equivalent resistance of the stack, and up to 10% of converted mechanical energy is dissipated in structural damping. These high losses are the result of the transient

response of the actuator, as shown in Figure 5.5 (a) and (b). The impulsive charge to the actuator causes an electrical oscillation of the stack at its resonance frequency.

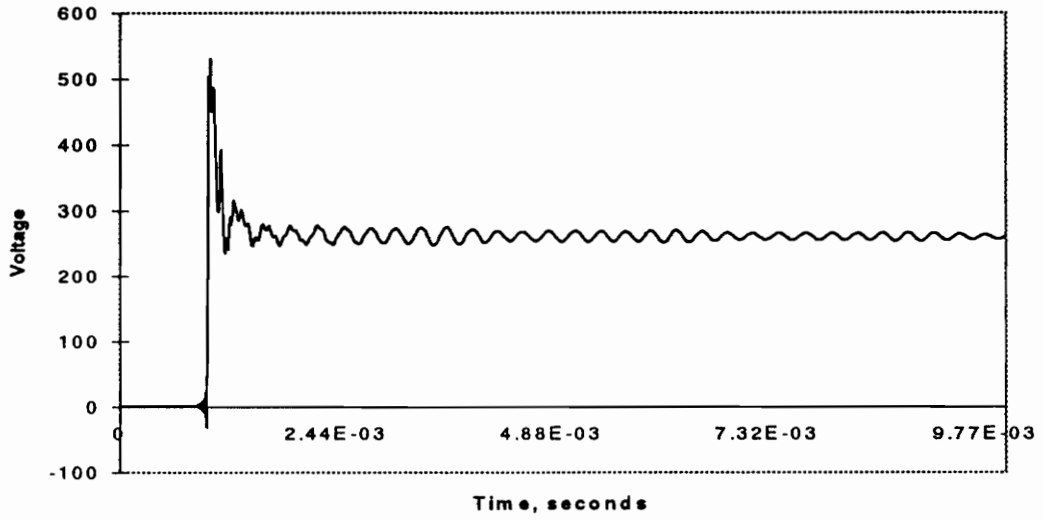

(a)

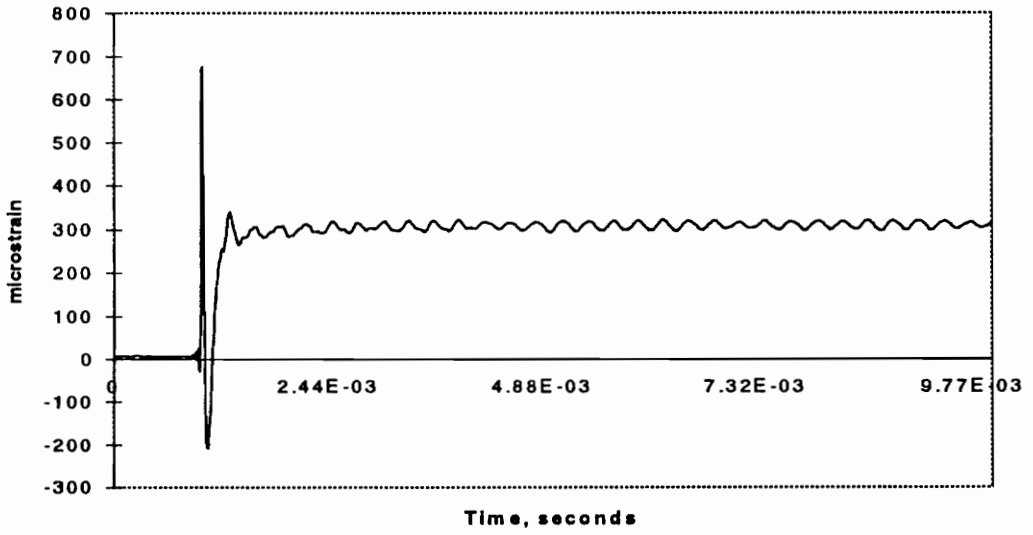

(b)

Figure 5.6 Transient response during impact; (a) voltage of actuator; (b) strain of actuator

The most energy dissipation occurs at the first few cycles and the dissipation continues for a fairly long time. This is just like a tuned damper that dissipates energy at the highest efficiency. Similarly, the PZT rod is also driven into a transient vibration, and part of the converted mechanical energy is lost in structural damping and acoustic radiation. This high dissipation occurs only under impulsive actuation.

For sinusoidal operation, unless operated at a resonance frequency, which is rarely the case for a stack actuator, the dissipation should be significantly lower. On the other hand, although the resonance oscillation and vibration dissipate a fairly large percentage of input energy, the overall efficiency may still be higher than at off-resonance frequency since the power factor is at its maximum. In fact, as the equivalent resistance of the PZT stack is typically small, the efficiency will be generally dominated by the power factor rather than the dissipation. Thus, for a capacitive actuator, the resonance or impulsive actuation is the most efficient operation mode. For the actuator being tested, about 34% of the input electrical energy is converted to mechanical energy, of which about 15-19%, including both the kinetic and strain, is useful for doing external work. Generally, the efficiency will be much lower than if the actuator is operated at non-resonance frequencies.

Table 5.3 also shows a noticeable dependency of the kinetic coefficient on the mass load. The highest coefficient, 0.166, is obtained for the 19-mm diameter ball. This is the result

of mechanical impedance matching. The 19-mm ball has a mass close to the effective mass of the stack (25 gram). A maximum amount of energy is transferred to the external structure when the internal and external impedance matches. A higher value might be obtainable if a perfect impedance match can be achieved.

Although most of the coefficients increase with the energizing voltage, the deviation is insignificant. This agrees with the fact that a PZT stack is linear within its working voltage range and the efficiency should be independent of the driving voltage.

The resonance-antiresonance method estimates the conversion efficiency of a rod PZT actuator by the following formula (Ikeda, 1990):

$$K_{33}^2 = \frac{\pi}{2}\frac{f_a}{f_r}\tan\left(\frac{\pi}{2}\frac{f_a - f_r}{f_a}\right), \tag{5.17}$$

where f_a and f_r are the antiresonance and resonance frequencies of a rod PZT actuator, respectively. For the stack actuator mounted on the test fixture, f_a and f_r are 3551 Hz and 3442 Hz, respectively, for the first mode, as shown in Figure 5.4. The corresponding coefficient is 7.8%, which is lower than K_s (=0.12), the ratio of the stored mechanical energy to the input electrical energy obtained above. It is assumed that Equation (5.17) underestimates the conversion efficiency in this dynamic case as the resonance-

antiresonance method essentially predicts the conversion coefficient under a static situation.

Summary

An experimental scheme for determination of the electromechanical conversion efficiency of a PZT stack actuator is presented. It is based upon a direct measurement of both electrical input energy and mechanical output energy and calculation of the conversion factor by definition. The results show that the overall efficiency of a PZT stack actuator with steel casing under impulsive actuation can be significantly lower than what its nominal coupling coefficient may imply. A substantial portion of input electric energy as well as converted mechanical energy is dissipated on the resistance of the stack and in structural damping as a result of transient response. The useful portion of the input energy, including kinetic and strain, seems no more than 20% in general. This value gives an upper bound of the efficiency of the stack. For sinusoidal actuation, although not directly investigated in this work, the coefficient is expected to be lower for any off-resonance frequencies.

Chapter 6

Conclusions and Recommendations

6.1 Conclusions

In this thesis, a novel approach of utilizing surface-bonded PZT active sensors or collocated sensor-actuators, along with measurement of coupled electric impedance, is presented. It provides a powerful non-intrusive tool for the acquisition of the structural dynamic or acoustic signature. As the core of the approach, a mathematical model governing the electromechanical interaction of the PZT actuator with the structure is derived, and explicit expressions for the mechanical mobility in terms of measured electric admittance are developed. The stiffening effect of the actuator on the structures is fully discussed and a solution is provided by use of mechanical impedance modeling. Two applications of the approach are presented in detail: structural modal analysis and structural health monitoring. As a general issue for PZT sensor-actuators in applications where a high power-to-weight ratio is critical, the electrical-to-mechanical energy conversion efficiency was experimentally investigated. The principle conclusions are as follows:

- An active PZT sensor is a device that can sense the structural response while conducting excitation through its piezoelectric effect. These functions may be carried out by use of an electric impedance analyzer.
- It is feasible to extract mechanical mobility from the measured electric admittance of active PZT sensors that are bonded to the structure under investigation. Due to the electromechanical interaction of the actuator with the structure, the electric admittance is modulated by the mechanical mobility (frequency response function) which may be extracted by a multi-input, multi-output model.
- The electric admittance approach provides an efficient and easy tool for acquisition of structural mobility. It reduces the number of transducers and the amount of instrumentation, simplifies the procedure, and reduces the costs compared to most other conventional methods.
- Acquisition of structural mobility through electric admittance is basically non-intrusive to the structure being tested, as the weight and stiffness of a PZT patch are usually negligible compared to that of the structure. This limited stiffening effect may be further removed by use of a mechanical impedance model if it is necessary.
- The electric admittance approach can be directly used for structural modal testing. The modal parameters, such as natural frequencies and modal damping, can be extracted from the electric admittance. The approach is especially suitable for structures that are light and flexible such that their modal parameters are extremely sensitive to the attachment of transducers.

- Active PZT sensors, along with electric admittance measurement, demonstrate an excellent feasibility for structural health monitoring. The deviation of coupled electric admittance is closely related to the structural integrity. The high sensitivity of the PZT sensor enables us to detect incipient damage in the structure with a minimal power requirement. The phenomenon of sensing localization allows for the determination of damage location in complex structures. However, ultrasonic frequency excitation is essential to the sensing localization.
- The temperature dependency of the PZT sensor may result in large errors when the PZT sensors are used for structural health monitoring. However, the errors can be effectively corrected by using a numerical approach based on the cross-correlation function.
- The overall energy conversion coefficient of a PZT stack actuator is found to be significantly lower than what the coupling coefficient implies. The major causes for this are the low power factor and the high electrical and mechanical dissipation during the actuation.

6.2 Recommendations

- The electric admittance approach for FRF extraction is a general method. It can be used for either 1-D structures, such as beams, or 2-D structures, such as plates. However, the model for the PZT sensor-actuator is one-dimensional. Unless the vibration modes of the structure are well-separated, which is not always the case for 2-

D structures, the electric admittance measured includes the contributions from two perpendicular directions, and the model may not be valid for the extraction of FRF for two-dimensional structures. If the approach is to be employed for plate or shell structures, a model of two-dimensional interactions needs to be developed such that the derived electric admittance of the sensor will include the flexural vibration modes along both directions of the structure.

- An analytical verification of the extracted in-plane mechanical mobility needs to be conducted by either finite element method or classical elasticity approaches.
- Although the scope of the sensing localization has been proven to be independent of the excitation level within the linear range of the structure, the effect of the voltage dependency of the PZT properties on the sensing reliability and sensitivity is not clear yet. Future work will involve the determination of the optimal excitation level for the highest signal-to-noise ratio of the structural signature and sensing scope with known structures. This will require an electric impedance analyzer with many higher levels of voltage output.

References

1. Agee, B., Zeng, X. and Michell L. D., "An Automated Mechanical Mobility Measurement System for Acquiring Data for Experimental Modal Analysis," *Proceedings of IMAC 10*, 3-7 Feb. 1992, San Diego, CA.
2. Bailey, T., and Hubbard, J. E., "Distributed Piezoelectric-Polymer Active Vibration Control of a Cantilever Beam", *Journal of Guidance, Control, and Dynamics*, Vol. 8, No. 5, 1985.
3. Bendat, J. S. and Piersol, A. G. " *Engineering Applications of Correlation and Spectral Analysis*", John Wiley & Sons, 1980, New York.
4. Bendiksen, O. O., " Mode Localization Phenomena in Large Space Structures", *AIAA Journal*, Vol. 25, No. 9, p. p. 1241-1248.
5. Bouzit, D. and Pierre, C., " An Experimental Investigation of Vibration Localization in Disordered Multi-Span Beams", *Proceedings of the 34th AIAA/ASME/ASCE/AHS/ASC Structures, Structural Dynamics, and Materials Conference, AIAA/ASME Adaptive Structures Forum*, part 3, La Jolla, CA, April 19-22, 1993, p. p. 1565-1577.
6. Crawley, E. F. and Anderson, E. H., " Detailed Models of Piezoceramic Actuation of Beam", *Journal of Intelligent Material Systems and Structures*, Vol. 1, 1990.
7. Chaudhry, Z. and Rogers, C. A., "The Pin-Force Model Revisited", *Journal of Intelligent Material Systems and Structures*, Vol. 5, No. 3, 1994.

8. Cole, D., Saunders, W. and Robertshaw, H., "The Dynamic Analysis of Piezostructures in Relation to Modal Analysis," *Proceedings of the 12th International Modal Analysis Conference (IMAC),* 1994, Vol. 1, p.p. 521-527.

9. Cole, D., Saunders, W. and Robertshaw, H., "Modal Parameter Estimation for Piezostructure," *Journal of Vibration and Acoustics*, 1995, Vol. 117, p.p. 431-438.

10. Dosch, J. J., Inman, D. J., and Garcia, E., "A Self-Sensing Actuator for Collocated Control," *ADPA Intl. Symposium. on Active Materials and Adaptive Structures*, Alexandria, VA, Nov. 1991.

11. Ewins, D. J, "Modal Test: Theory and Practice," Research Studies Press LTD., Letchworth, 1984, Hertfortshire, England.

12. Flint, E. Liang, C. and Rogers, C. A., "Electromechanical Analysis of Piezoelectric Stack Active Member Power Consumption", *Proceedings of the Second International Conference on Intelligent Materials*, 5-8 June, 1994, Colonial Willimsburg, VA.

13. Hagood, N. W. and Anderson, E. H., "Simultaneous Sensing and Actuation Using Piezoelectric Materials," *SPIE Conference on Active and Adaptive Optical Components*, July 1991.

14. IEEE standard on Piezoelectricity, ANSI/IEEE Std 176-1987.

15. Ikeda, T. "Fundamentals of Piezoelectricity," Oxford University Press, 1990, New York.

16. Lindner D. K. and Twitty G., "Damage Detection, Location, And Estimation for Large Truss Structures", *Proceedings of the 34th AIAA/ASME/ASCE/AHS/ASC*

Structures, Structural Dynamics, and Materials Conference, AIAA/ASME Adaptive Structures Forum, part 3, La Jolla, CA, April 19-22, 1993, p.p. 1539-1548.

17. Liang C., Sun F. P. and Rogers C. A., "Coupled electromechanical analysis of adaptive material system - Determination of the actuator power consumption and system energy transfer", *Journal of Intelligent Material Systems and Structures*, Vol. 5, No. 1, January 1994, p.p. 21-20.
18. Liang, C., Sun, F. P., and Rogers, C. A., "An Investigation of the Energy Consumption and Conversion of Piezoelectric Actuator Integrated In Active Structure," *Proceedings of the Second International Conference on Intelligent Materials*," 5-8 June, 1994, Colonial Willimsburg, VA, Technomic Pub. Co., Inc., Lanccaster, PA.
19. Okada, Y., Matsuda, K. and Hashitani H., "Self-sensing Active Vibration Control using the Moving Coil-Type Actuator," *Journal of Vibration and Acoustics*, 1995, Vol. 117, p.p. 411-415.
20. Peterson L.D. and Alvin K.F., "Damage detection using experimentally measured mass and stiffness matrices", *Proceedings of the 34th AIAA/ASME/ASCE/AHS/ASC Structures, Structural Dynamics, and Materials Conference, AIAA/ASME Adaptive Structures Forum*, part 3, La Jolla, CA, April 19-22, 1993, p.p. 1518-1528.
21. Physik Instrumente, "Products for Micropositioning," 1990.
22. Piezo Kinetics Incorporated, "Application Notes."

23. Sun, F. P., Liang, C. and Rogers, C. A., "Modal Analysis Using Collocated PZT Actuator/ Sensor-An Electromechanical Approach," *Proceedings of 1994 North American Conference on Smart Structures and Materials*, 13-18 February 1994, Orlando, Florida.

24. Sun, F. P., Liang, C. and Rogers, C. A., "Experimental Modal Testing Using Piezoceramic Patches As Collocated Sensor/Actuator," *Proceedings of 1994 SEM Spring Conference*, 6-8 June, 1994, Baltimore, Maryland.

25. Tavares R. and Kosmatka J. B., "Using Experimental Data to Detect Damage In Space Truss", *Proceedings of the 34th AIAA/ASME/ASCE/AHS/ASC Structures, Structural Dynamics, and Materials Conference, AIAA/ASME Adaptive Structures Forum*, part 3, La Jolla, CA, April 19-22, 1993, p. p. 1556-1564.

26. Sun F. P., Chaudhry Z., Liang C. and Rogers C. A. " Truss Structure Integrity Identification Using PZT Sensor-Actuator", *Proceedings of the 2th International Conference on Intelligent Materials,* , June 5-8, 1994, Colonial Williamsburg, VA, Technomic Pub. Co., Inc., Lanccaster, PA.

27. Stein, S., Liang, C. and Rogers, C. A., "Power Consumption of Piezoelectric Actuators in Underwater Active Structure Acoustic Control," *Proceedings of the 2nd Conference on Recent Advances In Active Control of Sound and Vibration*, April 28-30, 1993.

Appendix A Extracted mechanical mobility of a free-free aluminum beam

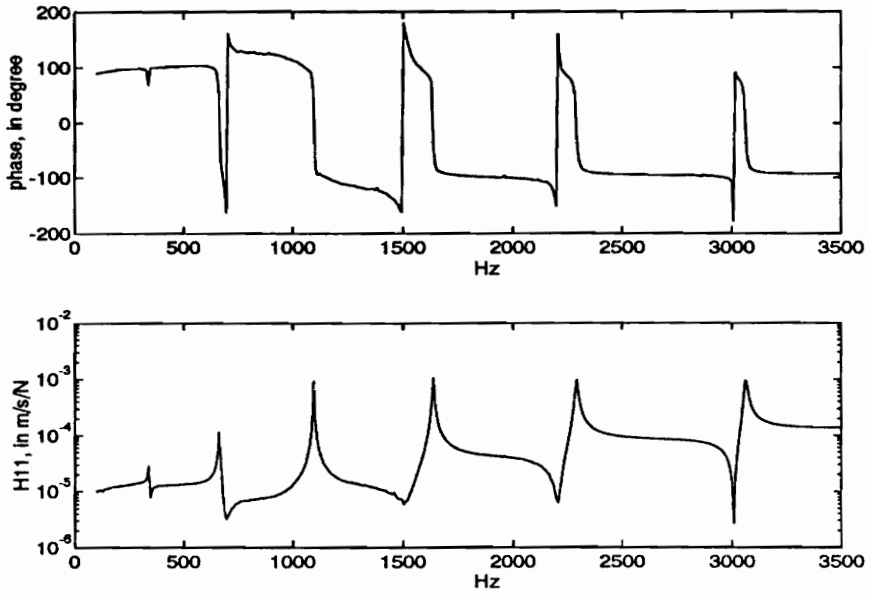

(a) H_{11}

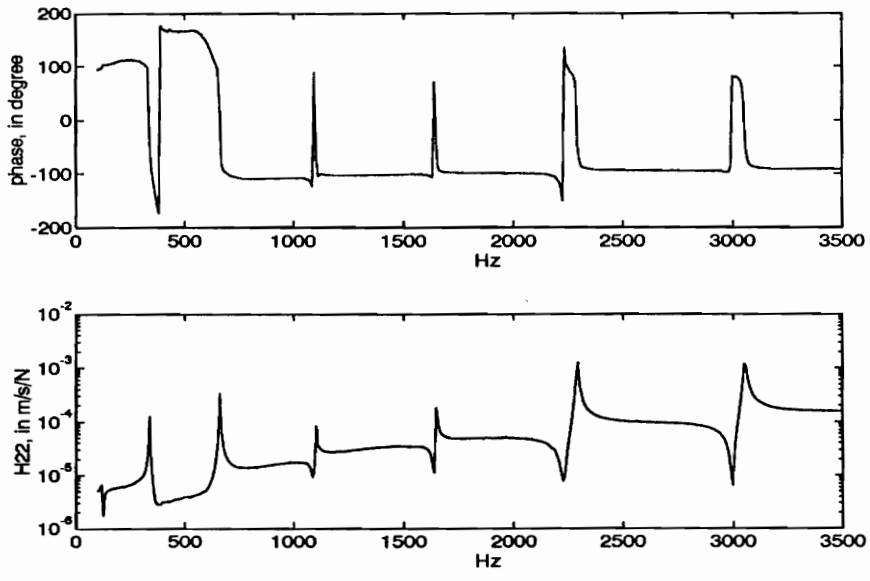

(b) H_{22}

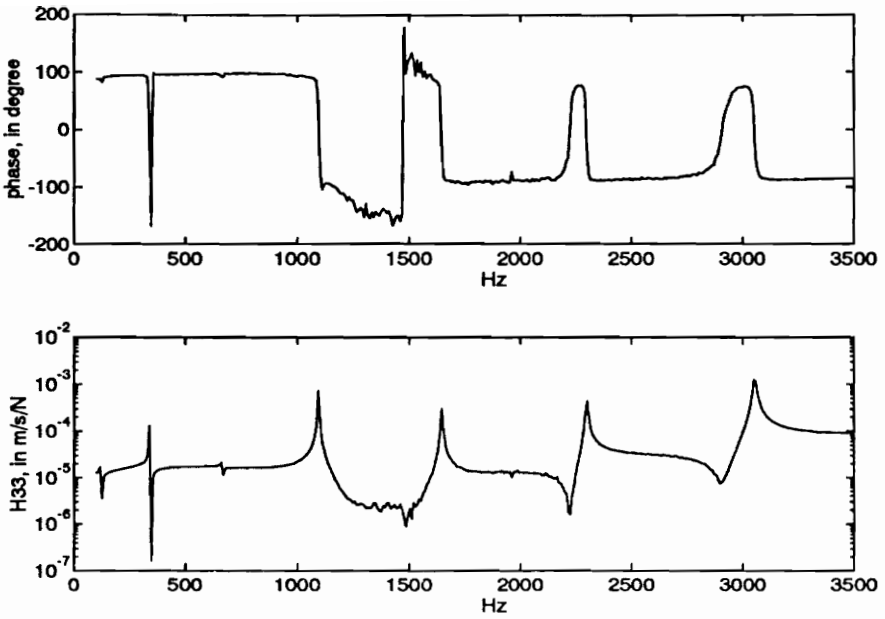
phase, in degree
200
100
0
-100
-200
0
500
1000
1500
2000
2500
3000
3500
Hz
H33, in m/s/N
10^{-2}
10^{-3}
10^{-4}
10^{-5}
10^{-6}
10^{-7}
0
500
1000
1500
2000
2500
3000
3500
Hz

(c) H_{33}

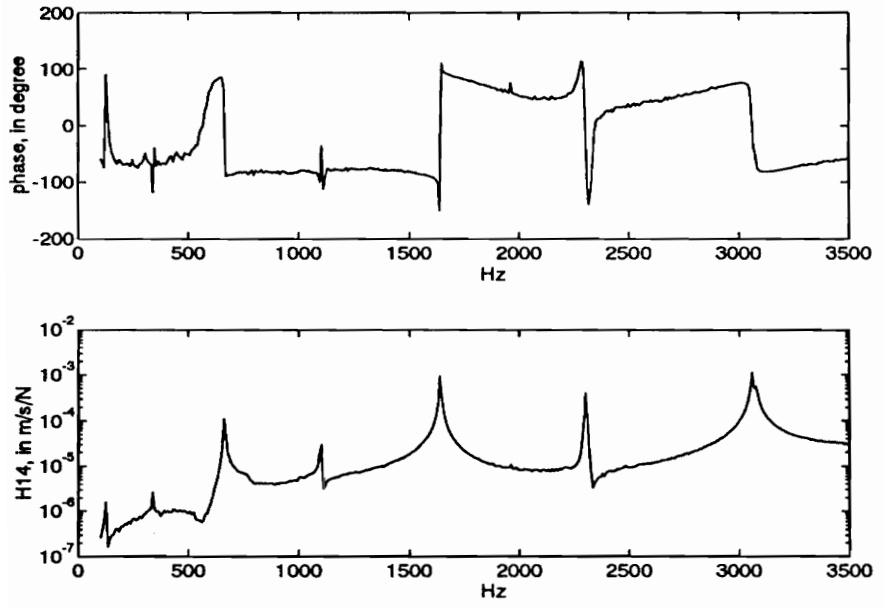
phase, in degree
200
100
0
-100
-200
0
500
1000
1500
2000
2500
3000
3500
Hz
H14, in m/s/N
10^{-2}
10^{-3}
10^{-4}
10^{-5}
10^{-6}
10^{-7}
0
500
1000
1500
2000
2500
3000
3500
Hz

(d) H_{14}

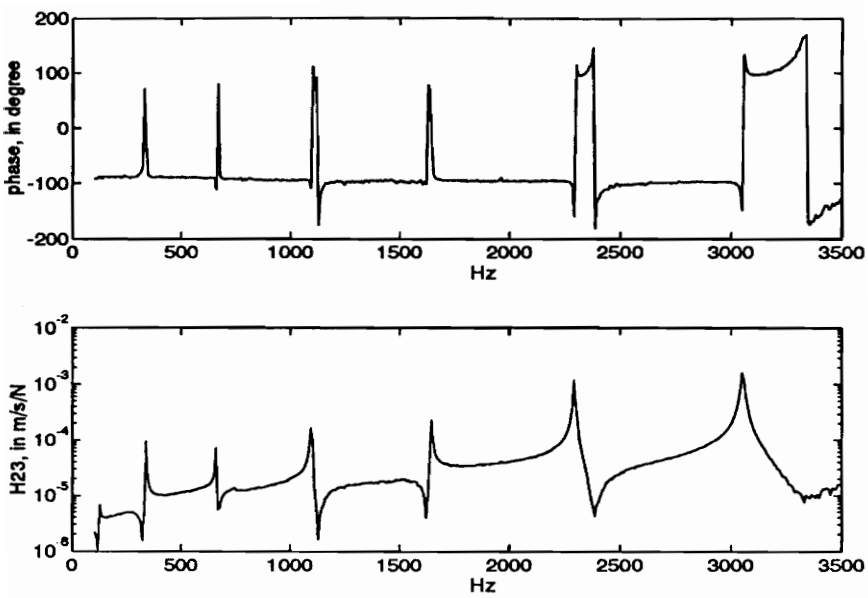
phase, in degree
200
100
0
-100
-200
0
500
1000
1500
2000
2500
3000
3500
Hz
H23, in m/s/N
10^{-2}
10^{-3}
10^{-4}
10^{-5}
10^{-6}
0
500
1000
1500
2000
2500
3000
3500
Hz

(e) H_{23}

Appendix B Electric admittance of a PZT active sensor mounted on the truss

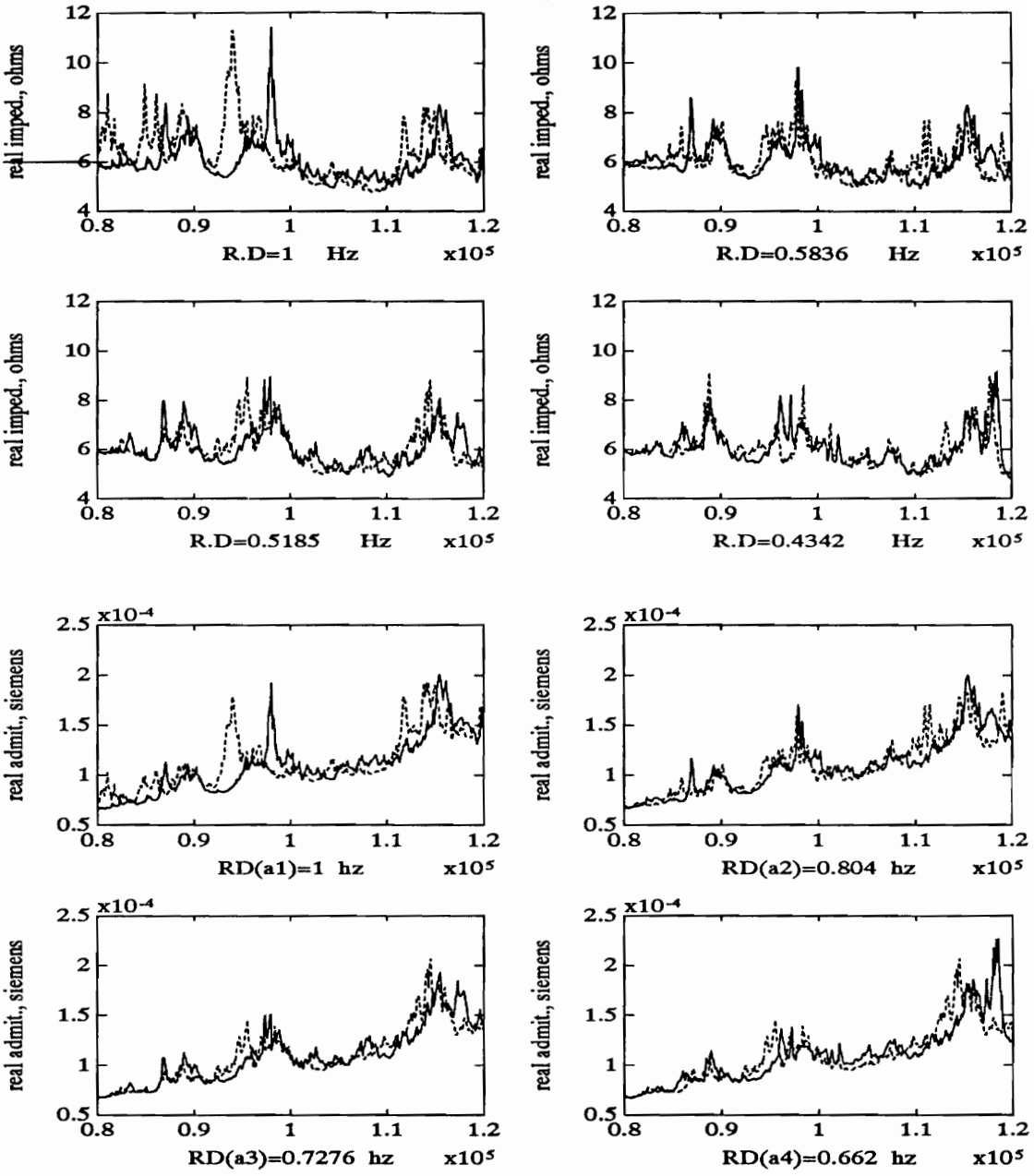

Node A

(The top four plots are the electric admittance when each of the struts at node A is slightly cut by a hacksaw. The bottom four are the admittance when each strut is loosened)

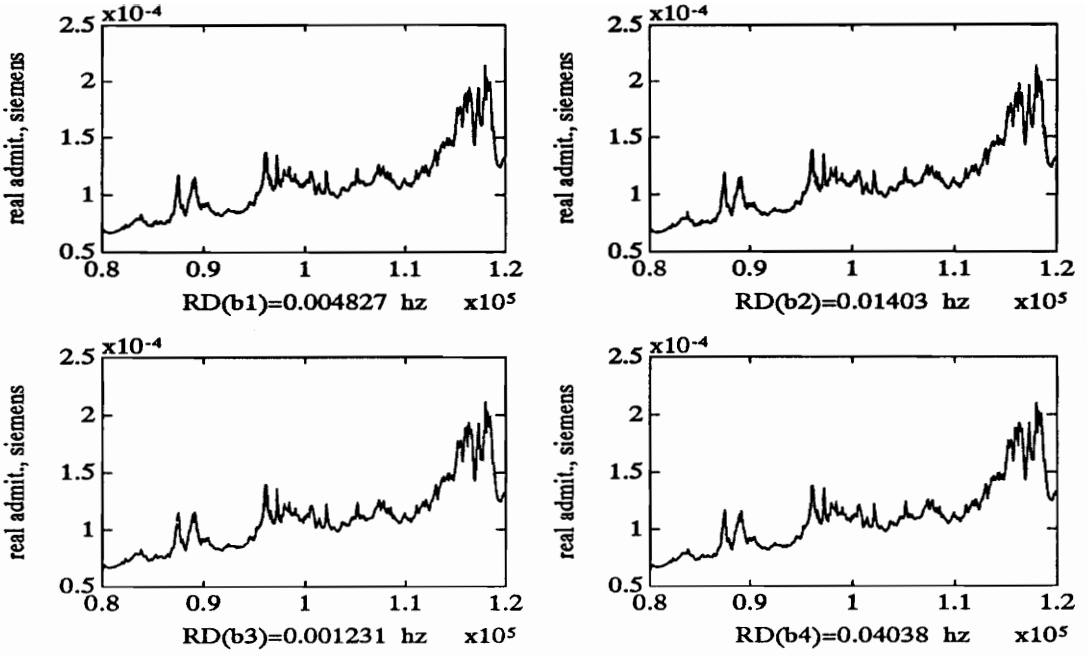

Node B
(The electric admittance when each strut at Node B is loosened)

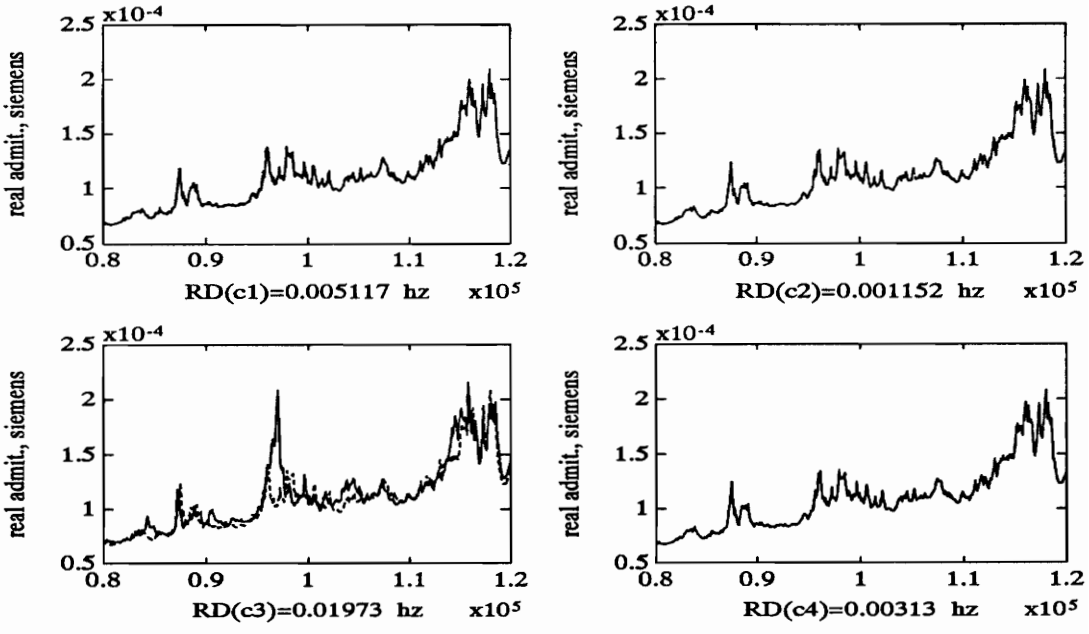

Node C
(The electric admittance when each strut at Node C is loosened)

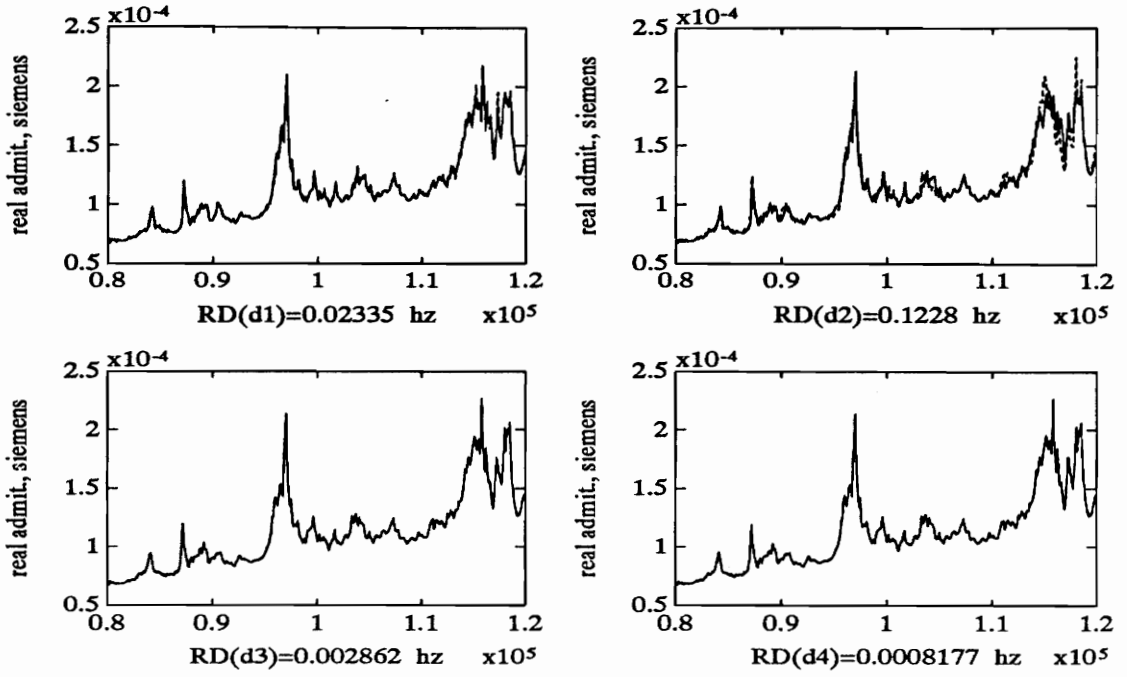

Node D

(The electric admittance when each strut at Node D is loosened)

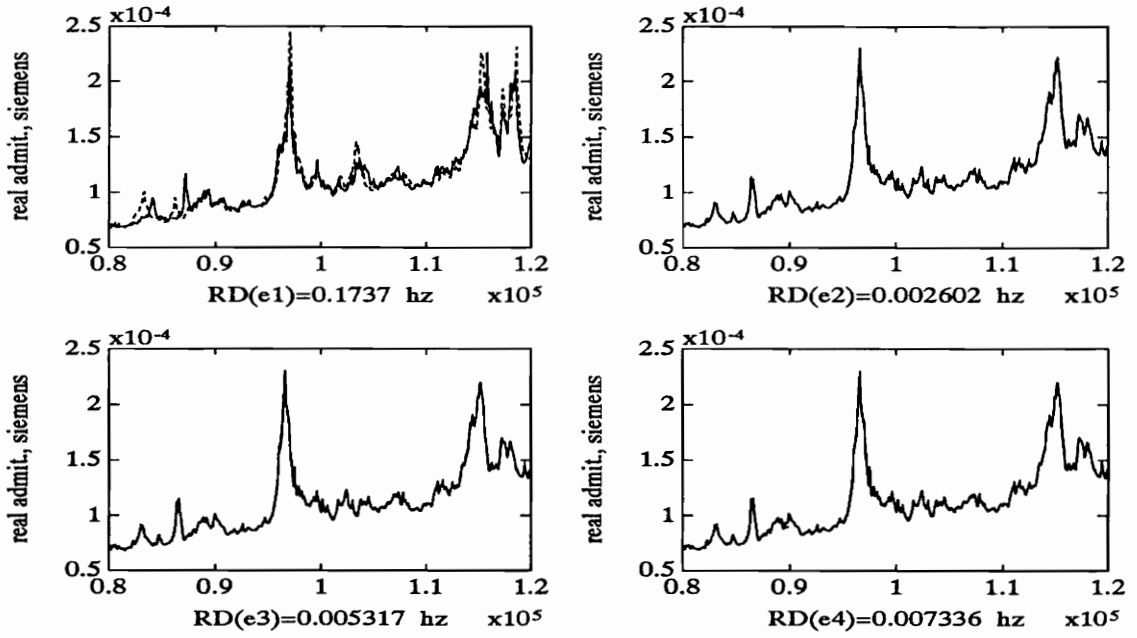

Node E

(The electric admittance when each strut at Node E is loosened)

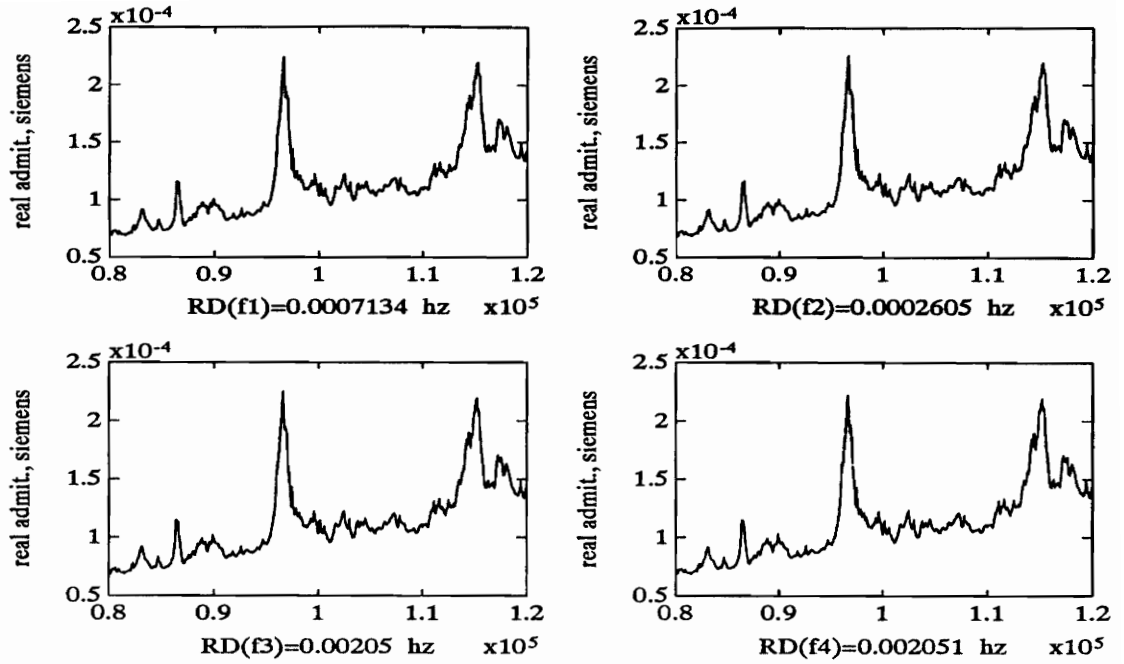

Node F

(The electric admittance when each strut at Node F is loosened)

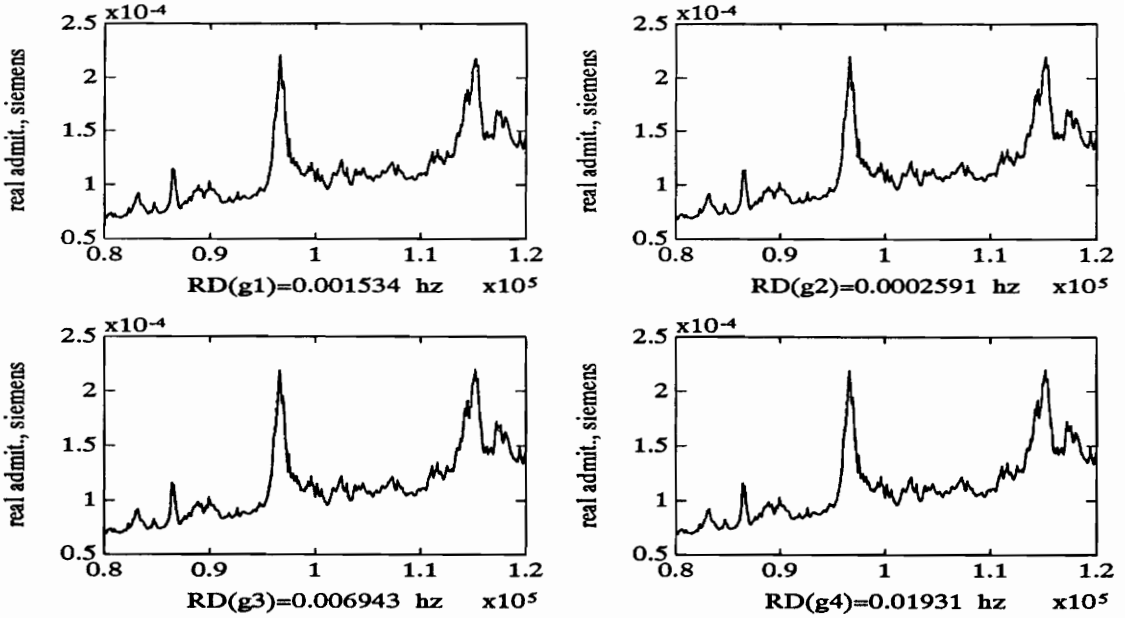

Node G

(The electric admittance when each strut at Node G is loosened)

Vita

Fanping Sun was born in Hangzhou, China on October 28, 1953. He obtained his Bachelor degree in Electronic and Mechanical Engineering from Zhejiang Institute of Silk Textiles in 1981 and his Master's degree in Mechanical Engineering from Zhejiang University in 1984. After that, he jointed Zhejiang Institute of Silk Textiles as a lecturer until he came to Virginia Polytechnic Institute and State University in 1991 as a Visiting Scholar. While working as a Research Associate at the Center for Intelligent Material Systems and Structures in 1994, he began part-time to pursue a Ph.D. degree. Mr. Sun is currently continuing to pursue his Ph. D. degree in Mechanical Engineering with emphasis on the intelligent structures.